ELSEVIER

Contents lists available at ScienceDirect

# **Quaternary Science Reviews**

journal homepage: www.elsevier.com/locate/quascirev





# Holocene hydroclimate variability of the Baltic region inferred from stable isotopes, *d*-excess and multi-proxy data at lake Nuudsaku, Estonia (NE Europe)

Mariliis Eensalu <sup>a,b,\*</sup>, Daniel B. Nelson <sup>c</sup>, Anna Buczynska <sup>a</sup>, Oliver Rach <sup>d</sup>, Tomi P. Luoto <sup>e</sup>, Anneli Poska <sup>b</sup>, Eric S. Klein <sup>f</sup>, Nathan D. Stansell <sup>a</sup>

- <sup>a</sup> Department of Earth, Atmosphere and Environment, Northern Illinois University, Dekalb, IL, 60115, USA
- <sup>b</sup> Department of Geology, Tallinn University of Technology, Tallinn, 19086, Estonia
- <sup>c</sup> Department of Environmental Sciences Botany, University of Basel, Basel, 4056, Switzerland
- d Helmholtz Centre Potsdam GFZ German Research Centre for Geosciences, Organic Surface Geochemistry Lab, Section 4.6: Geomorphology, Potsdam, 14473, Germany
- e Faculty of Biological and Environmental Sciences, Ecosystems and Environment Research Programme, University of Helsinki, Lahti, 15140, Finland
- f Department of Geological Sciences, University of Alaska Anchorage, Anchorage, AK 99508, USA

#### ARTICLEINFO

Handling Editor: A. Voelker

Keywords:
Biomarkers
Europe
Hydrogen isotopes
n-Alkanes
Quaternary
Organic geochemistry
Oxygen isotopes
Paleoclimatology
Plant wax
Relative humidity

#### ABSTRACT

Long-term hydroclimate records provide an opportunity to understand potential drivers of the past, and give context to modern and future climate warming. A wide variety of proxy data now allow for reconstruction of climate variables that were not previously possible. Here we present a multi-proxy dataset including n-alkane  $\delta^2 H$  ( $\delta^2 H_{n\text{-alk}}$ ) values from an open-basin lake in Estonia to reconstruct past hydroclimate conditions for the eastern Baltic region. We complement our sedimentary  $\delta^2 H_{n\text{-alk}}$  data with existing carbonate-based oxygen stable isotope ( $\delta^{18}O$ ) data to derive deuterium (d-) excess. We present multiple isotopic records and reconstructed relative humidity ( $\Delta RH$ ) values over the Holocene, and link these with modern precipitation  $\delta^2 H$  and  $\delta^{18}O$  values to guide the interpretation of the paleo-proxies. Fossil pollen and chironomid-based temperature reconstructions, as well as biogeochemical data provide additional information for inferring past environmental changes. Our results indicate that the middle Holocene in Estonia had on average  $6\pm 3\%$  higher RH values than the late Holocene. The  $\delta^{18}O$  and  $\delta^2 H$  values were also higher during the middle Holocene, which we interpret as increased warm season precipitation. Our reconstructed d-excess values were relatively higher during the middle Holocene, indicating a more northerly or cold source water origin, in comparison to the late Holocene. In addition to the paleoclimatic significance, our results show how multiple quantitative proxies can be combined to characterize hydroclimate sensitivity to changes in relative humidity, temperature and moisture source.

#### 1. Introduction

#### 1.1. Hydroclimate in the Baltic region

Global temperatures during modern times have been rising at an unprecedented rate (IPCC, 2019), causing increased rainfall, severe weather events and droughts, and changes in the seasonality of precipitation (Rosenzweig and Neofotis, 2013). Climate models predict significant change in global climate over the next century, and the Baltic region in northern Europe could experience up to ~15% rise in precipitation (Räisänen, 2016). However, climate models show high

uncertainty regarding the magnitude of possible future change (Trenberth, 2011). These future projections rely on analogous data of past climate change, however a recent study by Bova et al. (2021) demonstrated that reconstructions of mean annual conditions are not fully descriptive of past climates. Russo and Cubasch (2016) also argue that the amplitude of past climatic changes in the models in Europe is incorrect. The confidence of the models predicting future climate change can be improved by examining long-term (centennial to millennial-scale) climate mechanisms and processes from periods that experienced warm conditions similar to today (Bracegirdle et al., 2019).

The Baltic region is a prime area to better comprehend past ocean-

<sup>\*</sup> Corresponding author. Department of Earth, Atmosphere and Environment, Northern Illinois University, Dekalb, IL, 60115, USA. *E-mail address:* meensalu@niu.edu (M. Eensalu).

atmosphere processes and their potential thresholds. Estonia, in particular, lies in a zone that is sensitive to cold arctic airmasses during the winter months, yet experiences relatively warm summers. Observed modern precipitation and temperature patterns in the Baltic region are well associated with shifts in North Atlantic sea-surface temperatures and coupled atmosphere-ocean dynamics (Rummukainen et al., 2001). While modern precipitation patterns demonstrate the importance of seasonal changes on local hydroclimate (Bonfils et al., 2004), it is currently unclear how hydroclimate in the Baltic region responded to seasonal distribution of solar insolation and to ocean-atmospheric circulation changes on millennial timescales.

#### 1.2. Research questions

Temperature reconstructions based on pollen records are in agreement that the northern European summers were generally warmer in the middle Holocene (from 8200 to 4200 cal yrs BP) than in the late Holocene (from 4200 cal yrs BP to present), however, greater uncertainty is associated with the hydrological conditions during these time intervals (Wanner et al., 2008). It is possible that the balance of seasonal precipitation during the Holocene shifted in response to declining warm season and increasing cold season insolation. The available proxy records suggest that although the middle Holocene in northern Europe was likely drier overall, there might have been greater seasonality in precipitation, making winters wetter and summers drier than today (Guiot et al., 1993; Mauri et al., 2014; Russo and Cubasch, 2016). Some studies have argued that Holocene hydroclimatic shifts were driven more by changes in cold season moisture source and less by temperature (Charman et al., 2009; Persoiu et al., 2017; Surić et al., 2021). It has also been suggested that the middle Holocene was dominated by enhanced zonal flow (Perșoiu et al., 2017) implying that the annual hydroclimatic conditions in Europe during the middle Holocene could have been relatively wetter instead of drier (Lauterbach et al., 2011). Conversely, the Atlantic Meridional Overturning Circulation (AMOC) likely experienced weakening during the Holocene that would have resulted in decreasing westerly air mass flow, and therefore more arid conditions (Hammarlund et al., 2002). These uncertainties can be addressed by developing new proxy records that we use here to quantitatively reconstruct hydroclimatic and atmospheric circulation variables.

# 1.3. Lake sediment proxies - theory

Lake sediments are excellent proxies to help resolve the questions related to past hydroclimate due to their capacity to continuously record environmental signals at a relatively high temporal (in most cases decadal to centennial) resolution (Leng and Marshall, 2004). Oxygen  $(\delta^{18}O)$  and hydrogen  $(\delta^{2}H)$  stable isotope records preserved in lake sedimentary biomarkers provide an opportunity to track changes in paleo-precipitation using multiple information sources, and past atmospheric moisture cycling (Henderson-Sellers et al., 2004). To date, there are only a few well-dated Holocene-spanning lacustrine oxygen isotope records from the Baltic region (Veski et al., 2004; Laumets et al., 2014; Stančikaite et al., 2015; Stansell et al., 2017; Street-Perrott et al., 2018). The records provide long-term information about local and regional-scale hydroclimate dynamics in Estonia with a broad perspective of past circulation changes across the region. However, cases where  $\delta^{18}O$  and  $\delta^{2}H$  proxies have been studied in the same lake basin are scarce, and a detailed investigation of the combined effects of effective moisture and past air mass origins remains unexplored.

Estimating the changes in the  $\delta^2 H$  of paleo-precipitation ( $\delta^2 H_{paleo-precip}$ ) using a multi-proxy approach can provide insight to hydrological history of a region. The  $\delta^2 H$  of precipitation ( $\delta^2 H_{precip}$ ) undergoes a series of isotope fractionations before storing the precipitation signal in a leaf wax biomarker such as the  $\delta^2 H$  value in n-alkanes ( $\delta^2 H_{n-alk}$ ), which are refractory compounds forming in plant leaves. The leaf water used as the hydrogen source to form long-chain n-alkanes (n-C<sub>25</sub> – n-C<sub>33</sub>) carries

information about the plant's source water and relative humidity (Sachse et al., 2004; Aichner et al., 2017). Once the available water is taken up by the plant and transported to leaves, leaf transpiration in terrestrial plants includes a significant offset, which also varies as a function of relative humidity (RH) and temperature, and has been evaluated as  $49.4\pm7.2\%$  at our specific field site (Eensalu et al., 2023). Furthermore, the RH varies regionally and is often higher in forests than in the surrounding areas at a given site. Based on a recent study conducted on Estonian plants, the apparent fractionation ( $\epsilon_{app}$ ), which describes the net effect between  $\delta^2 H_{precip}$  and  $\delta^2 H_{n-alk}$ , is  $-92\pm21\%$  on average for all n-alkanes (Eensalu et al., 2023).

Mid-chain n-alkanes (n- $C_{17} - n$ - $C_{23}$ ) typically dominate in aquatic plants and algae (Ficken et al., 2000; Aichner et al., 2010; Gao et al., 2011). Despite this generalization, these compounds can also be produced in lower quantities by terrestrial plants, in appreciable quantities by some types of Sphagnum, and in other cases aquatic plants have been shown to produce few alkanes with chain lengths shorter than n-C<sub>23</sub> (Pancost et al., 2003; Bush and McInerney, 2013; Aichner et al., 2017; Berke et al., 2019; Eensalu et al., 2023). Nevertheless, when an aquatic origin can be supported, short/mid-chain length alkane  $\delta^2$ H values from compounds such as n- $C_{23}$  have been applied as tracers of a non-isotopically enriched precipitation isotope signal (Rach et al., 2014, 2017). This approach rests on the assumption that the primary source water for the plants that synthesize the majority of these compounds found in a sediment record is representative of local precipitation without alteration by evaporation, or by transpiration within leaves exposed to dry air prior to biosynthesis. Aquatic plants growing in a lake with open basin hydrology meet these requirements. Although this is not as clearly the case for plants that may grow nearby the lake, such as *Sphagnum*, in this case we note that *Sphagnum* lipid  $\delta^2$ H values have been shown to be insensitive to wet vs dry growth regimes (Brader et al., 2010). Unfortunately, n-alkanes are not highly source-specific biomarkers, but despite this, general patterns in co-variation among *n*-alkane abundances and  $\delta^2$ H values within a sediment record can be leveraged to improve interpretations of sedimentary records provided that data from multiple compounds are available. For example, changes in n-C<sub>23</sub> abundance or  $\delta^2$ H values that closely track changes in more unambiguous terrestrial plant compounds such as n-C29 or n-C31 may indicate a major terrestrial source for n-C23, while uncorrelated changes may support interpreting an aquatic plant origin for n-C23. Provided that an appropriate aquatic source interpretation can be made, in an open-basin lake such as Nuudsaku (Fig. 1), mid-chain n-alkanes (specifically n- $C_{23}$ ) provide a means for reconstructing past precipitation isotope information (Brader et al., 2010; Rach et al., 2014; Stansell et al., 2017). When paired with data from unambiguous terrestrial plant markers such as n-C29, the data can be combined to estimate past changes in humidity (Rach et al., 2017).

Relative humidity (in addition to temperature) impacts the  $\epsilon_{app}$  values in terrestrial plants (Cernusak et al., 2016). Until recently, the mechanisms behind the processes influencing the relative humidity changes ( $\Delta$ RH) in sedimentary archives were challenging to assess as there was a lack of methods that allowed for a direct and quantitative reconstruction of past hydrological dynamics. Although our knowledge of processes affecting the transport and deposition of biomarkers is still limited, and several assumptions accompany even the most up to date methodologies, the modeling advancement by Rach et al. (2017) demonstrated that a dual-biomarker approach is an effective means for inferring quantitative  $\Delta$ RH values from lipid biomarkers. This method uses pollen data to account for changes in the vegetation distribution in the sedimentary  $\delta^2 H_{n-alk}$  values, and chironomid proxy to account for changes in the paleotemperature.

Paleo-lake water  $\delta^{18}O$  values, and past precipitation  $\delta^{18}O$  ( $\delta^{18}O_{paleo-precip}$ ) can be inferred from the  $\delta^{18}O$  of authigenic calcite ( $\delta^{18}O_{calc}$ ) proxy (Talbot, 1990; Leng and Marshall, 2004). Authigenic calcite precipitation in the lake water captures the lake water  $\delta^{18}O$  signal, but also includes temperature-dependent isotope fractionation (Sharp, 2007),

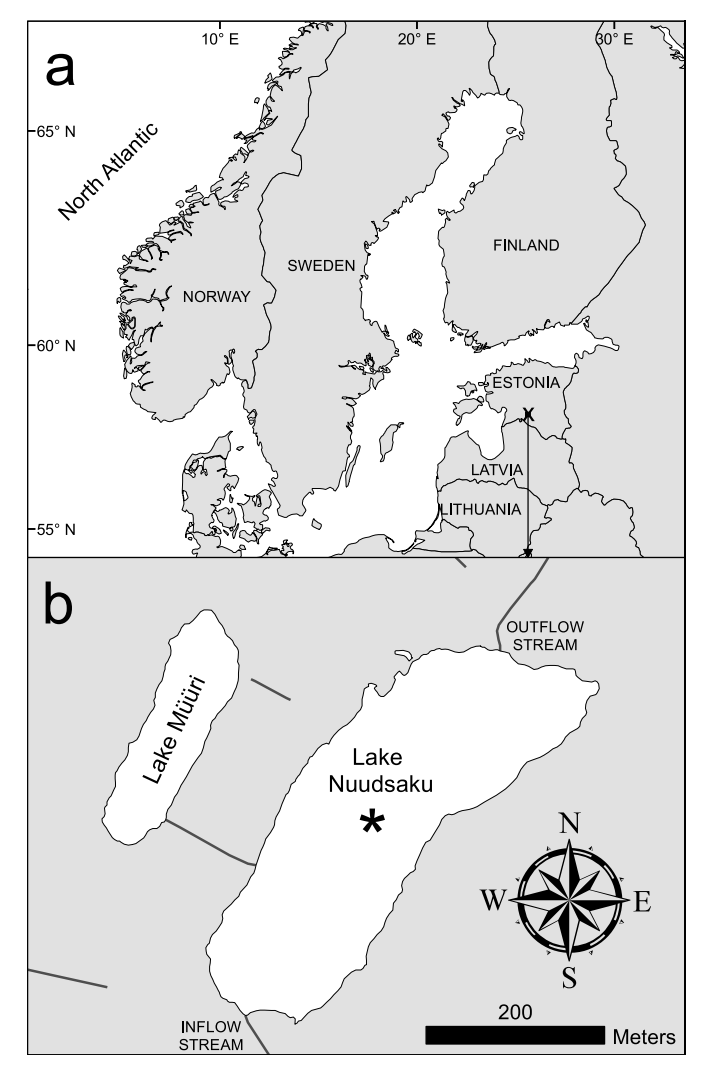


**Fig. 1.** Map of Europe in top panel (a) where the x in Southern Estonia represents the location of Lake Nuudsaku. Asterisk in the middle of Lake Nuudsaku in bottom panel (b) marks the approximate sediment coring location.

which can bias the lake water signal in the absence of a temperature correction. For example, the lake Nuudsaku record from Estonia is likely sensitive to both temperature and precipitation changes, and the hydroclimate interpretation based on the  $\delta^{18} O_{calc}$  signal would benefit from an independent temperature proxy.

Chironomid (Diptera: Chironomidae) head capsules and pollen assemblages in the lake sediments can be used as proxies of past temperatures (Seppä and Poska, 2004; Luoto and Nevalainen, 2009). The larvae of various chironomid (non-biting midge) species are sensitive to environmental conditions and prefer to live at different temperatures and water depths. Once the larvae develop into pupae, the unique larvae head capsules are shed during summer months, deposited and well-preserved within lake sediments (Luoto et al., 2020). The warm season temperature record inferred from chironomid assemblages can serve as a tool for calculating past calcite to water fractionation factors (Kim and O'Neil, 1997), which facilitates quantitative reconstructions of past lake water  $\delta^{18}O$  values from  $\delta^{18}O_{calc}$  values. Pollen records commonly identify local vegetation changes on the landscape in response to climatic, environmental, and also anthropogenic variables, such as crop growing, increasing landscape openness, and herding (Seppä et al., 2004). As a widely used quantitative method, pollen proxies provide a great amount of detail about the development of an area as each vegetative species has a different preference and range of temperatures, light conditions, pH, nutrient availability and moisture

regimes (Felde and Birks, 2019).

Although each informative in their own right, interpreting  $\delta^2 H_{paleoprecip}$  and  $\delta^{18} O_{paleoprecip}$  records together can provide an enhanced view into past hydrological changes. Deuterium excess (*d*-excess) is a second-order parameter calculated from the stable water isotopes (*d*-excess =  $\delta^2 H - 8 \times \delta^{18} O$ ) which carries information about the origin of the moisture source that is not apparent with either isotope in isolation (Dansgaard, 1964; Jouzel et al., 2005). For example, there are equilibrium and kinetic isotope fractionations for both oxygen and hydrogen isotopes when water is evaporated to vapor that leave a distinct imprint on the combined isotope signal of the resulting vapor (Dansgaard, 1964; Klein et al., 2015; Klein and Welker, 2016). Subsequent atmospheric transport and rainout effects generally result only in equilibrium isotope effects while preserving the kinetic isotope-based offset between  $\delta^2 H$  and  $\delta^{18} O$  values that was stored at the point of evaporation, which can be described by the *d*-excess value (Gat, 1996).

# 1.4. Current study

We developed records using the proxies described above in Lake Nuudsaku sediments to help resolve questions relating to hydroclimate and atmospheric circulation in the Baltic region since the early Holocene (~9500 cal yrs BP). With this approach, we reconstructed  $\Delta$ RH and isotopic fractionation between terrestrial and aquatic n-alkanes based on  $\delta^2$ H values. We calculated d-excess and developed complementary datasets using pollen, chironomids, and stable carbon and nitrogen isotopes to provide a new perspective on the timing and patterns of Holocene hydroclimate dynamics in the eastern Baltic region. We specifically set out to contextualize these reconstructed hydroclimate shifts, and provide quantitative values for past  $\Delta$ RH, and calculated the d-excess with the purpose of increasing our understanding of the potential changes in moisture sources.

#### 2. Study site

#### 2.1. Lake location and surroundings

Lake Nuudsaku (Fig. 1) is an open-basin lake located in the center of Sakala Upland in Viljandi County, southern Estonia (58°11'49" N,  $25^{\circ}37'40''$  E). The lake lies  $\sim$ 90 m above sea level with a surface area of  $\sim$ 8 ha, maximum water depth of  $\sim$ 5.1 m and a catchment area of  $\sim$ 6.2 km<sup>2</sup>. A small stream (5.1 km; slope declination of 1.86 m/km) flows through the lake from south to north, and a stream originating from an adjacent spring-water fed Lake Müüri flows to Lake Nuudsaku from the west. The lake water turnover time is ~1 year. Lake Nuudsaku is surrounded by fens, which are abundant in graminoids, not Sphagnum moss. Aquatic plants can be found on most of the shores as well as in the deeper parts of the lake. Water chemistry measurements from July 2019 show that Lake Nuudsaku dissolved organic carbon (DOC), inorganic carbon (IC), total carbon (TC) and total nitrogen (TN) concentrations were 0.5, 5.3, 5.8 and 1.1 mg/L, respectively. Measurements from the Nuudsaku stream conducted at the same time resulted in 0.0 mg/L DOC, 7.0 mg/L IC, 6.9 mg/L TC and 1.9 mg/L TN.

Lake Nuudsaku typically freezes over during the winter months. There is a small campground near the lake, and no roads are in close proximity of the lake except for the local private courtyard. The lake basin consists of Quaternary deposits on top of Devonian sandstone (Mäemets, 1968). Local vegetation around Lake Nuudsaku is best described as a mix of (Euro-Siberian) boreal coniferous and deciduous forests. The local plants mostly photosynthesize between April and October as Estonia lies in the northern part of the temperate climate zone (Jaagus and Ahas, 2000).

# 2.2. Local climate conditions

Estonian climate is shaped by both maritime and continental climate

(Jaagus, 2009). Precipitation in Estonia mostly originates from the North Atlantic Ocean, but a small fraction comes from the Mediterranean and Black Sea areas of the Balkans (Mätlik and Post, 2008; Gimeno et al., 2013). Annual precipitation at Lake Nuudsaku (Viljandi Meteorological station) is ~715 mm, of which ~ 75% is lost to evapotranspiration (Fig. 2). Based on measurements from 2011 to 2020 at the Viljandi station, the cold season (Nov–Apr) precipitation makes up ~ 300 mm and warm season (May–Oct) ~ 420 mm. Average cold season temperature is -0.4 °C and warm season temperature 13.5 °C (Estonian Meteorological Survey, https://www.ilmateenistus.ee/kliima/ajalool ised-ilmaandmed/). The average monthly evaporation at Lake Nuudsaku is ~45 mm/month and ~540 mm/year, 350 mm in summer and 190 mm in winter (modeled using R package Evapotranspiration (Guo et al., 2016) with hourly air pressure, precipitation, temperature, dew point, wind speed, relative humidity and solar radiation data from 2011

to 2020 provided by the Estonian Meteorological Survey). Evapotranspiration exceeds precipitation from March to May.

#### 2.3. Climate drivers

The North Atlantic Oscillation (NAO) is a dominant mode of variability affecting northern European hydroclimate, defined by an atmospheric pressure gradient between the Icelandic Low and the Azores High (Hurrell and Van Loon, 1997). Strong positive phases result in higher precipitation amounts over northern Europe due to below-normal air pressure at high latitudes, which is most pronounced during winter months, however correlation between the modern-day NAO and precipitation during summer months is negative (Hurrell et al., 2003; Luoto and Helama, 2010). The negative phase of NAO is a result of lower-than-average difference between the Azores High and

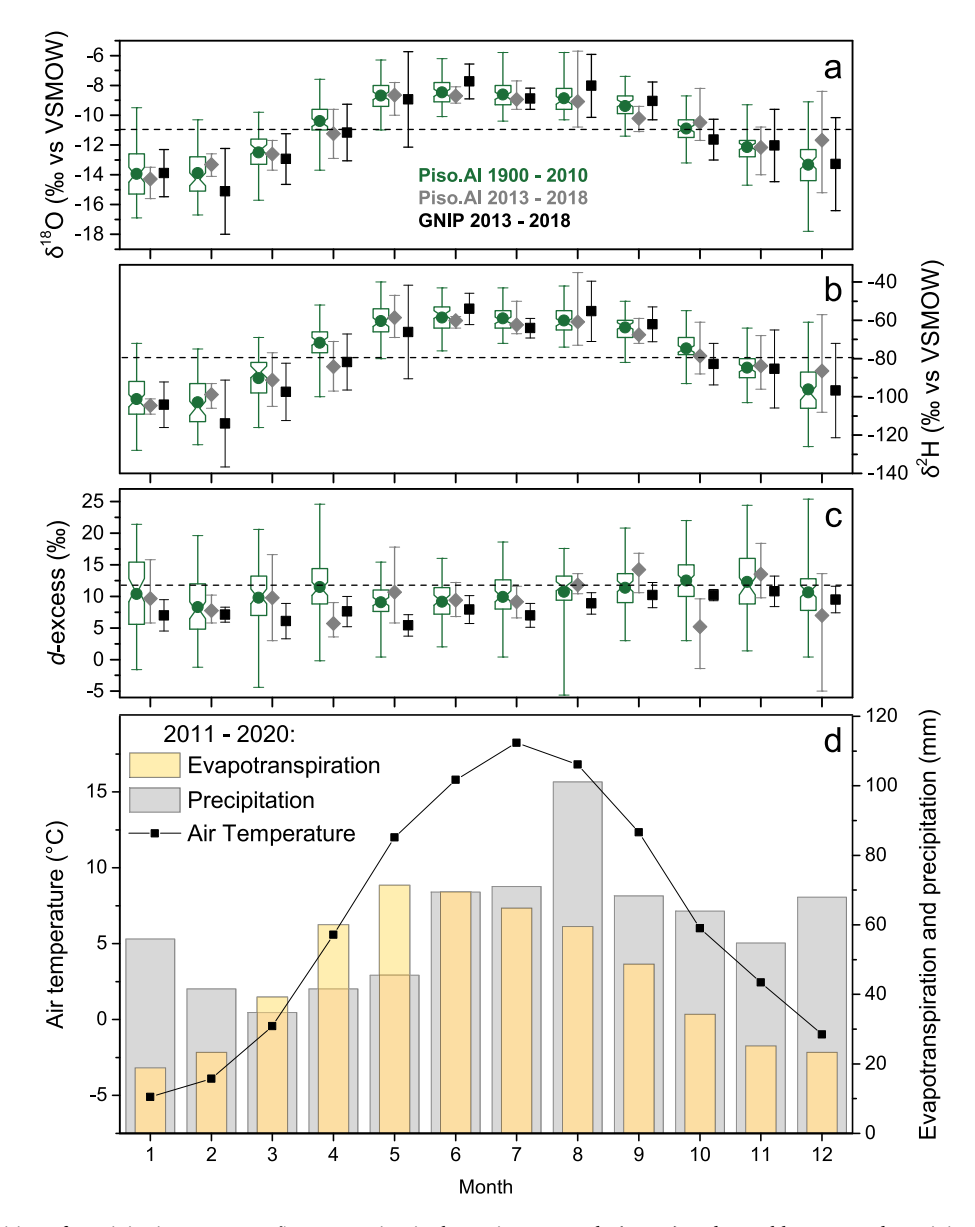


Fig. 2. Isotopic composition of precipitation at Tartu-Tōravere station is shown in top panels (a to c) and monthly measured precipitation and modeled evapotranspiration amounts in the bottom panel (d). Precipitation  $\delta^{18}O$  (a),  $\delta^{2}H$  (b) and d-excess (c) data with error bars at the GNIP Tartu-Tōravere monitoring station (58°15′51″ N, 26°27′41″ E) from 2013 to 2018 are shown as black squares with mean yearly values represented by black horizontal dashed lines. Green notched and gray boxes represent modeled Piso.AI data at Tartu-Tōravere from 1900 to 2010 and from 2013 to 2018, respectively. Bottom plot (d) shows average monthly precipitation and air temperature data (2011–2020) acquired from Viljandi meteorological station (http://www.ilmateenistus.ee/kliima/), accompanied by modeled evapotranspiration rates (R package Evapotranspiration) based on the same data set.

Icelandic Low, a condition which is characterized by cold and dry conditions in northern Europe, and warm and wet conditions in southern Europe (Lamb and Peppler, 1987). The positive phase of NAO, on the contrary, is characterized by above-average pressure differences between the subtropical high and sub-polar low, which in turn, results in an intensified Atlantic jet stream that brings warmer and wetter conditions to the northern, and colder and drier conditions to southern Europe (Lamb and Peppler, 1987).

The Scandinavian pattern (SCP) teleconnects the north Atlantic and the climate of continental Europe (Barnston and Livezey, 1987). This sub-seasonal climate index is a measure of the relative north to south atmospheric pressure gradient across Europe. A 55-year reanalysis study by Wang and Tan (2020) demonstrates that a positive (negative) phase of SCP is associated with anticyclonic (cyclonic) conditions and dry (wet), below (above)-average temperatures and precipitation over Scandinavia and western Russia.

# 2.4. Modern isotopes in precipitation

The instrumental  $\delta^{18} O_{precip},~\delta^2 H_{precip}$  and d-excess values at the Tartu-Tōravere station in Estonia between 2013 and 2018 (Fig. 2) range from -20.26% to -4.75% (mean -11.00%), -154.5% to -33.1% (mean -79.8%), and 2.90% to 14.24% (mean 8.25%), respectively. The Piso.AI (Nelson et al., 2021) modeled  $\delta^{18} O_{precip},~\delta^2 H_{precip}$  and d-excess values from 1900 to 2020 at the same location range from -18.8% to -5.6% (mean -11.0%), -132% to -41% (mean -80.0%), and -8.4% to 24.2% (mean 7.72%), respectively. Modeled values from 2013 to 2018 range from -15.6% to -5.9% (mean -8.0%), -116% to -44% (mean -77.5%), and between -8.4% and 18.4% (mean 8.0%) for  $\delta^{18} O_{precip}, \delta^2 H_{precip}$  and d-excess, respectively (Fig. 2). The warm and cold season d-excess mean values calculated from the instrumental data,

are 8.0% ( $1\sigma = 2.4\%$ ) and 8.5% ( $1\sigma = 2.7\%$ ), respectively. The 1900 to 2020 data from Piso.AI results in *d*-excess mean values of 8.1% ( $1\sigma = 4.3\%$ ) during warm seasons and 7.4% ( $1\sigma = 4.8\%$ ) during cold seasons.

#### 3. Methods

#### 3.1. Lake water sampling and analyses

Water samples from southern Estonian lakes (n = 62), rivers/streams (n = 13) and bogs (n = 13) were collected during summer months between July 2019 and July 2022 (Supplemental Table 1). The water isotope data are plotted (Fig. 3) with previously published data (Stansell et al., 2017) and Estonian spring and well data (Raidla et al., 2016). Water samples were measured for  $\delta^{18}O$  and  $\delta^{2}H$  in the Klein Lab at the University of Alaska Anchorage, All water samples were screened prior to analysis to avoid any organic matter contamination during the analyses, and none of the samples in this study needed filtering. Each water isotope sample was analyzed on a L2130-i or Picarro L2140-i water isotope analyzer. The measurement precision for the samples in this study was  $\pm 0.2\%$  for  $\delta^{18}$ O and  $\pm 2\%$  for  $\delta^{2}$ H, and repeat measurements of the USGS 45 (-2.2%  $\delta^{18}$ O and -10.3%  $\delta^{2}$ H vs Vienna Standard Mean Ocean Water, or VSMOW) and USGS 46 (-29.8%  $\delta^{18}$ O and -235.8% $\delta^2$ H vs VSMOW) standards were used to verify these precision ranges. Each sample was injected six times. The first three injections of each sample were excluded due to potential memory effects, and the mean of the last three injections was used to calculate the water isotope value. All isotope results for this study are reported in per mil (%) notation and calculated using the equation of  $\delta = \frac{R_{sample}}{R_{standard}} - 1$  where the R represents the ratio of the abundance of heavy isotope to the light isotope (Coplen, 2011).

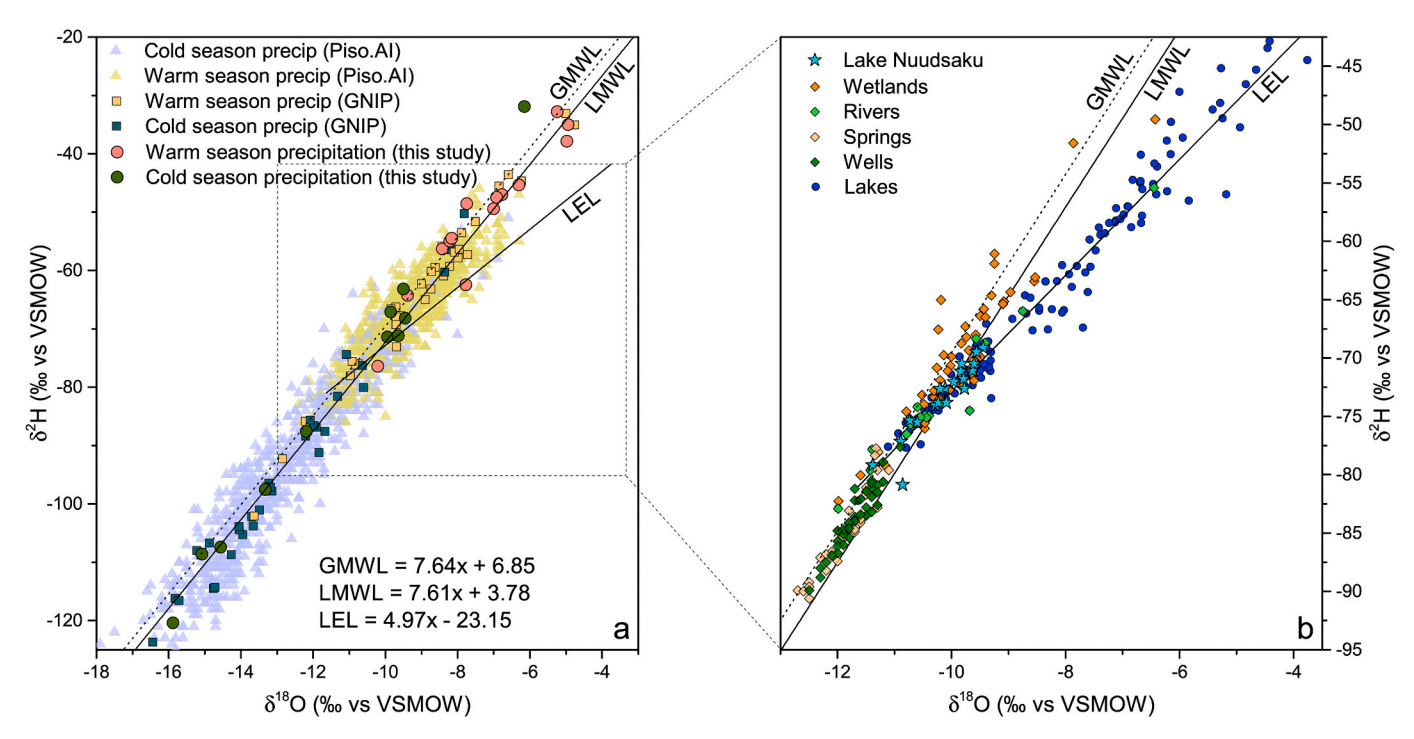


Fig. 3. Modern surface and meteoric water  $\delta^{18}O$  and  $\delta^{2}H$  values from Estonia. Warm (May to October) and cold (November to April) season precipitation isotopes are shown in the left panel. Lines represent the regional meteoric water line (LMWL), local evaporation line (LEL) and global meteoric water line (GMWL, y = 7.64x + 6.85; Putman et al., 2019). LMWL was calculated from modeled Piso.AI (1900–2020; Nelson et al., 2021), Global Network of Isotopes in Precipitation (GNIP) reported at Tartu-Tōravere meteorological station (2013–2018) and precipitation water data by Stansell et al. (2017), which are also plotted on panel a. Blowout of the left panel (a) is the right panel (b), showing Estonian well and spring data by Raidla et al. (2016), and wetland, river and lake water isotope results from the current study (Supplemental Table 1) as well as by Stansell et al. (2017). The LEL is a linear fit through Estonian lake water isotope data (n = 205) from this study and by Stansell et al. (2017). (For interpretation of the references to color in this figure legend, the reader is referred to the web version of this article.)

#### 3.2. Sediment sampling, processing, and chronology

Lake Nuudsaku sediment cores were collected from the deepest part of the lake (58°11′49″N, 25°37′39″E; Fig. 1) during the summer of 2014 using a modified Livingston piston corer, and transported to the lab in polycarbonate tubes. Lake Nuudsaku sediment core collection in the field, sedimentology, bulk geochemistry and endogenic sedimentary carbonate stable isotopes are described in detail by Stansell et al. (2017). Furthermore, the lake sediment cores were scanned with a smartcube® Camera Image Scanner SmartCIS. The existing radiocarbon chronology (Stansell et al., 2017) was improved by measurements from four new samples, which were pretreated and combusted at Northern Illinois University. The samples were then converted to graphite and measured at the W.M. Keck Carbon Cycle AMS Laboratory at the University of California Irvine. The age-depth model was developed using the IntCAL20 calibration curve (Reimer et al., 2020) and BACON package in R (Blaauw and Christen, 2018). All ages discussed are modeled calibrated years before 1950 CE (cal yrs BP).

# 3.3. Chironomid fossil assemblage analysis and temperature reconstruction

The chironomid fossil assemblage analyses of Lake Nuudsaku sediments was performed as described in Luoto et al. (2020). Briefly, sample preparation and analyses involved sieving the untreated (without KOH pre-treatment) wet sediment samples (n = 39) through a 100- $\mu$ m mesh to remove all fine-grained sediment material. Chironomid head capsules were then extracted with fine forceps under a stereo microscope at a 25x magnification and mounted on microscope slides. Chironomids were identified under a light microscope at 100 to 400x magnification according to Brooks et al. (2007) with a target counting sum set to 50 individuals. The chironomid-inferred mean July temperature (CI-TJul) reconstruction was carried out using the East European calibration model (Luoto et al., 2019) that was constructed as described by Luoto et al. (2020). The temperature range in the calibration set is 11.3-20.1 °C from 212 sites and it includes 142 chironomid taxa. Chaoborids are not included the temperature calibration set, and therefore do not contribute to the temperature reconstruction. Chironomid and Chaoborus community diversity indices were estimated using Hill's (1973) N2 effective number of occurrences.

#### 3.4. Carbon and nitrogen abundance and isotope analyses

The stable isotopes of carbon ( $\delta^{13}$ C) and nitrogen ( $\delta^{15}$ N) from dry bulk sediment (n = 13) were measured on Elemental Combustion System (ECS 4010, Costech Instruments) coupled with the Delta Plus Advantage IRMS (Thermo Fisher Scientific) at Northern Illinois University. Aliquots of each sample were measured before acidification to obtain  $\delta^{13}$ C values of total carbon ( $\delta^{13}$ C<sub>bulk</sub>), % total carbon (TC),  $\delta^{15}$ N values and % total nitrogen (TN). Subsequently, additional sample aliquots were acidified by fumigation with concentrated HCl (according to Harris et al., 2001) to obtain  $\delta^{13}$ C values of organic carbon ( $\delta^{13}$ Corg) and % total organic carbon (TOC). Seven samples were additionally acidified directly with 1 N HCl. The difference in  $\delta^{13}\text{C}$  between fumigated and directly acidified samples was between 0.01 and 0.15%. The isotopic values were calibrated using two reference standards for both carbon and nitrogen. These standards were selected to bracket the range of the values in analyzed samples. In-house standards were previously calibrated with the use of NBS-22 oil and IAEA-CH-6 sucrose (carbon) and USGS-25, IAEA-N1 (nitrogen). One of the in-house standards included Acetanilide, a commercially available standard calibrated at Indiana University as one of the anchors for both nitrogen (+19.56  $\pm$  0.03‰) and carbon ( $-29.5 \pm 0.02\%$ ) (Schimmelmann et al., 2009). These standards were run in the beginning and end of each sequence. Quality control standard was run every 12 samples. The ratio of % Total Organic Carbon (TOC) over % Total Nitrogen (TN) was then calculated (C/N

ratio) by multiplying the result by their atomic ratio of 1.167 (Meyers and Lallier-Vergès, 1999). Relative proportions of the terrestrial vs aquatic organic matter were calculated following standard procedure (Ishiwatari et al., 2009). The average C/N values of 20 and 6 were estimated for terrigenous (TOC/TN $_{\rm terr}$ ) and aquatic (TOC/TN $_{\rm aq}$ ) organic matter, respectively.

#### 3.5. Lipid biomarker (n-alkane) extraction and quantification

Lake Nuudsaku sediment was subsampled at ~300-year intervals (n = 30) from a previously acquired composite core (Stansell et al., 2017) and the samples were freeze dried. Dry samples weighed between 3 and 14.3 g, and were spiked with 50  $\mu$ g of  $5\alpha$ -androstane. Samples in capped Erlenmeyer vials were placed in Fisher Scientific FS30 Ultrasonic bath three times for 20 min with 30 ml of 9:1 v/v dichloromethane/methanol (DCM/MeOH). The resulting Total Lipid Extract (TLE) was pipetted off the sediments after every sonication and then filtered using 55 mm diameter 0.45 µm Whatman glass microfiber GF/A filters and Wheaton 0.45 μm PTFE filters. The *n*-alkane aliphatic fraction was separated from the TLE using activated silica gel (VWR high purity irregular, 40–60 µm, 60 Å) on a Solid Phase Extraction block (Supelco Visiprep™) using 12 ml of hexane. Sulphur particles and unsaturated compounds were removed using 6 ml of hexane on activated copper (<425 µm Aldrich) columns and activated AgNO<sub>3</sub> coated silica gel (+230 mesh), respectively. Urea adduction was performed on all samples to remove the remaining cyclic and branched compounds after biomarker quantification on a gas chromatograph coupled with a mass spectrometer (GC-MS). Samples were concentrated under Organomation Associates, Inc. N-EVAP<sup>TM</sup>111 Nitrogen Evaporator and stored airtight in 1.5 ml amber vials.

The sedimentary n-alkanes were identified and quantified using a GC-MS (QP2010S, Shimadzu Scientific Instruments, Kyoto, Japan) at Northern Illinois University. For quantification we used an n-C<sub>7</sub>-C<sub>40</sub> alkane standard (1000 µg/ml each component in hexane, Supelco, Sigma Aldrich, MO, USA) along with 5α-androstane (Sigma Aldrich, MO, USA) as an internal standard. The DB5-MS column (Agilent Technologies, 30 m length, 0.25 mm i.d., and 0.25  $\mu$ m film thickness) was used to separate the compounds with a splitless injection at 290 °C. The GC temperature was kept at 60 °C for 1 min, followed by a temperature gradient of 10 °C/min to 170 °C, and afterwards, of 4 °C/min to 300 °C. Out of the 30 samples analyzed, 7 were run in duplicates. Relative standard deviation (RSD) was generally below 10% for all analytes, exceeding that value in 8% of cases. The average RSD was 3.7%. Percent error between expected and calculated amounts for calibration standards at three different concentration levels (calculated for *n*-alkanes in the range of n- $C_{17}$  to n- $C_{35}$ ), which were treated as unknows, was below 24% (7 injections, at the beginning, in the middle and at the end of the measurement sequence).

#### 3.6. Stable hydrogen isotope analysis of sedimentary n-alkanes

Hydrogen stable isotope analyses were made using a gas chromatograph coupled with a High Temperature Conversion oven and an isotope ratio mass spectrometer (GC-HTC-IRMS) system (Trace GC Ultra interfaced to a MAT253, Thermo Scientific, Bremen, Germany). Compounds were separated on a DB5-MS column (Agilent Technologies, 30 m length, 0.25 mm i.d., and 0.25 µm film thickness), for which a spitless injection was used for 2 min at 280 °C. The GC temperature was kept at 70 °C for 3 min, followed by a temperature gradient of 10 °C/min to 150 °C, and afterwards, by a gradient of 4 °C/min to 320 °C. The High Temperature Conversion (HTC) oven was kept at 1420 °C. The  $\delta^2$ H values were normalized to the VSMOW scale using a mixture of n-alkanes obtained from Indiana University. Stable hydrogen isotope ratios of these standards were measured off-line according to Schimmelmann et al. (1999) at Indiana University. The H<sub>3</sub><sup>+</sup> factor was measured before every major sequence run. Samples were run before and after the procedure of urea adduction. For samples that were run before the

adduction procedure, the internal standard was used as a quality check. The  $\delta^2H$  of  $5\alpha$ -androstane was  $-249.8\pm3.5\%$ , calculated from a set of 86 injections from a period of two months. The measurement precision  $(1\sigma)$  of 6  $\emph{n}$ -alkane compounds  $(\emph{n}\text{-}C_{23}$  to  $\emph{n}\text{-}C_{29})$  in calibration standard was between 3.0 and 4.1% for 88 injections done over the period of two months, and these were treated as unknows which were not included in the normalization procedure. The difference between calculated value and the certified value was between 1.2 and 3.4% for 5  $\emph{n}\text{-}$ alkanes and 8.3% for an  $\emph{n}\text{-}$ alkane for which the  $\delta^2H$  value was outside of the calibration range. The values of all  $\emph{n}\text{-}$ alkanes extracted from the sediment samples analyzed in this study were within the calibration range of  $\delta^2H$  values used for scale correction procedure.

#### 3.7. Proxy-derived variables

The measured *n*-alkane data were used to calculate several variables. Carbon preference index (CPI) characterizes the relative abundance of odd over even *n*-alkane chains (Bray and Evans, 1961) and was calculated using the formula:

$$CPI = \frac{1}{2} \times \left( \frac{\sum \frac{C_{23-31}^{odd}}{\sum C_{22-30}^{oven}} + \frac{\sum C_{23-31}^{odd}}{\sum C_{24-32}^{oven}} \right)$$
 (1)

The n-C $_{17}$  and n-C $_{18}$  content was often below the detection limit, hence these are not included in the CPI calculation. Average carbon chain length (ACL) describing changes in vegetation was calculated as follows (Eglinton and Hamilton, 1967):

$$ACL = \frac{\sum C_i \times i}{\sum C_i}$$
 (2)

where i represents carbon chain length from n- $C_{23}$  to n- $C_{33}$  (Poynter and Eglinton, 1990). The ACL value of the surface-most sediment was acquired from Eensalu et al. (2023).

The proportion of aquatic plants in the n-alkane content ( $P_{aq}$ ) was estimated using equation (3) (Ficken et al., 2000):

$$P_{aq} = \frac{C_{23} + C_{25}}{C_{23} + C_{25} + C_{29} + C_{31}}$$
(3)

Hydrogen isotopic fractionation between terrestrial ( $\delta^2 H_{terr}$  from n- $C_{29}$ ) and aquatic ( $\delta^2 H_{aq}$  from n- $C_{23}$ ) n-alkane derived  $\delta^2 H$  ( $\epsilon_{2Hterr/aq}$ ) was calculated using equation (4) (Rach et al., 2017):

$$\varepsilon_{2Hterr/aq} = \left(\frac{\delta^2 H_{terr} + 1}{\delta^2 H_{aq} + 1}\right) - 1 \tag{4}$$

The grouping of terrestrial vs aquatic *n*-alkane chains was decided based on hierarchical cluster analysis which is a method used to hierarchically partition variables based on their dissimilarity to one another (Revelle, 1979). In case of a missing *n*-C<sub>23</sub> alkane  $\delta^2 H$  ( $\delta^2 H_{C23}$ ) value in sediment sample data, the  $\delta^2 H_{aq}$  values were inferred from the  $\delta^2 H_{C25}$  value (n = 3).

We reconstruct the quantitative change in % relative humidity ( $\Delta$ RH) from  $\delta^2$ H<sub>C23</sub> following Rach et al. (2017):

$$\Delta RH = \left(\frac{\varepsilon_{2Hterr-aq}}{-e_{sat} \times (\varepsilon_{+} + \varepsilon_{k})} + \frac{1}{e_{sat}}\right) \times 100\%$$
 (5)

where the  $e_{sat}$  represents the saturation vapor pressure,  $\epsilon_+$  the equilibrium isotope fractionation between liquid and vapor and  $\epsilon_k$  is the kinetic isotope fractionation from intercellular leaf water to atmosphere. The  $e_{sat}$  and  $\epsilon_+$  are both function of temperature, which was calculated using our CI-TJul values after Rach et al. (2017). Atmospheric pressure value of 1001.65 hPa at 90 m above sea level was also incorporated in calculating the  $e_{sat}$  values. We corrected the Lake Nuudsaku  $\epsilon_{2Hterr/aq}$  values by calculating the relative amount of grasses vs trees (Feakins, 2013; Rach et al., 2017) in a nearby Lake Päidre pollen profile (Saarse et al., 1995). We used the average relative amount of grasses vs trees

(7.74% vs 92.26%) from  $\sim$ 8500 to  $\sim$  1250 cal yrs BP as an input variable after  $\sim$  1250 cal yrs BP in the Lake Nuudsaku data set as Lake Päidre sedimentary record only spans from early Holocene up to  $\sim$  1250 cal yrs BP (details below). We assumed that air the temperature was equal to CI-TJul values from our Lake Pangodi record with a mean error of 1.17 °C.

Plant physiological parameters in our  $\Delta RH$  model ( $g_s$  and  $r_b$ , which were used to calculate  $\epsilon_k$ ) were input according to Eensalu et al. (2023). The previously calculated modern peak summer time  $g_s$  (stomatal conductance) values in Estonia range from 0.07 to 0.09 with an error range of 0.006 mol m $^{-2}s^{-1}$  (Eensalu et al., 2023). Boundary layer resistance ( $r_b$ ) in modern plants was estimated to be 1.0 m $^2$  s mol $^{-1}$ , as suggested by previous studies (Jones, 2013; Rach et al., 2017). We used the variance of  $\pm 0.006$  mol m $^{-2}s^{-1}$  for  $g_s$  and  $\pm 0.05$  m $^2$  s mol $^{-1}$  for  $r_b$  to estimate the range in the  $\Delta RH$  values. See Rach et al. (2017) for details. Since this method cannot be used to calculate absolute changes in RH, we normalized the  $\Delta RH$  model output to the modern (from 2010 to 2014, which is 5 years prior to the sediment collection) RH value of 80.5%. We assumed that the top sediment would represent  $\sim$ 5 years in the record, and the % values of  $\Delta RH$  presented are therefore in comparison to modern values.

The Lake Nuudsaku  $\delta^{18}O_{calc}$  proxy from the same core (Stansell et al., 2017) was converted from the Vienna Pee Dee Belemnite (VPDB) to the VSMOW scale using formula 6 (Kim et al., 2015):

$$\delta^{18}O_{calc}(VSMOW) = \alpha_{calc/w} \times \delta^{18}O_{(VPDB)} + 30.92\%$$
 (6)

Chironomid-inferred July temperatures (CI-Tjul) were used to calculate calcite/water fractionation factors ( $\alpha_{(calc/w)}$ ) using formula 7 (Kim and O'Neil, 1997):

$$1000~ln~\alpha_{(calc/w)} = 18.03 \times \frac{10^3}{T} - ~32.42 \approx \alpha_{calc/w} - 1 = \epsilon_{calc/w} \eqno(7)$$

where the T (in K) is represented by CI-TJul values. Mean July temperatures were used in particular because carbonate deposition in Estonia is the highest during summer months as a result of abundant photosynthetic algae (Laugaste and Lessok, 2004). The  $\epsilon_{calc/w}$  was then applied to the calcite-derived  $\delta^{18}O$  to calculate for the lake water  $\delta^{18}O$  ( $\delta^{18}O_{lakewater}$ ) which we interpret as  $\delta^{18}O_{paleo-precip}$  (VSMOW):

$$\delta^{18}O_{paleoprecip} = \left(\frac{\delta^{18}O + 1}{\varepsilon_{calc/w} + 1}\right) - 1 \tag{8}$$

The  $\textit{n-C}_{23}$  alkanes were not abundant enough in our surface sediment to measure the  $\delta^2H_{C23}$  value. Based on regime shift analyses, the available  $\delta^{18}O_{calc}$  record (Stansell et al., 2017) does not suggest any major changes in the late Holocene. Therefore, we infer the mean  $\delta^2H$  values of paleo-precipitation ( $\delta^2H_{paleo-precip}$ ) for the topmost sediment from the Piso.AI model results (-80.7%,  $1\sigma=18.0\%$ ) spanning from 1901 to 2020 (Nelson et al., 2021), which is similar to the instrumental GNIP record (-79.8%,  $1\sigma=23.2\%$ ) from 2013 to 2018 (IAEA, 2022). In other words, we assume that our most recent  $\delta^2H_{C23}$  value (-168.3%,  $1\sigma=6.8\%$  from 191 years ago) is reasonably consistent with the mean conditions from 1901 to 2020. Applying an apparent isotope fractionation ( $\epsilon_{app}$ ) of -95% to this  $\delta^2H_{C23}$  value results in a  $\delta^2H_{precip}$  value of 81.0%. This is in agreement with the Piso.AI mean precipitation  $\delta^2H$  value from the past 120 years, so we use this to calculate  $\delta^2H_{paleo-precip}$  values for the Lake Nuudsaku record, as shown in equation (9).

$$\delta^2 H_{paleoprecip} = \left(\frac{\delta^2 H_{C23} + 1}{\varepsilon_{C23/w} + 1}\right) - 1 \tag{9}$$

Deuterium excess (d-excess) was calculated using formula 10:

$$d - excess = \delta^2 H_{paleoprecip} - 8 \times \delta^{18} O_{paleoprecip}$$
 (10)

The combination of  $\delta^2 H$  terrestrial and aquatic data, and  $\delta^2 H$  aquatic and  $\delta^{18} O$  aquatic data rely on temporal synchroneity of the proxy data and a lack of seasonal bias. However, the lake and soil water at

Nuudsaku integrate the precipitation  $\delta^2H$  and  $\delta^{18}O$  signal over time, smoothing out the seasonal cycle. The modern annual evaporation (Fig. 2) was modeled using the R package Evapotranspiration (Guo et al., 2016) with Estonian Weather Service from 2011 to 2020 hourly temperature, precipitation, dew point, solar radiation, average wind speed, relative humidity and air pressure data measured at the Tartu-Tōravere meteorological station. The monthly precipitation water isotope  $(\delta^{18}O_{precip})$  and  $\delta^2H_{precip})$  data spanning from 2013 to 2018 was provided by the same station (IAEA, 2022). The Piso.AI model v1.2020 (downloaded on January 03, 2022) was used to predict  $\delta^{18}O_{precip}$ ,  $\delta^2H_{precip}$  and d-excess values at Nuudsaku (Nelson et al., 2021). The prediction errors were  $\pm 1.9\%$  for  $\delta^{18}O_{precip}$  and  $\pm 14.5\%$  for  $\delta^2H_{precip}$ .

All data were projected to a uniform age scale using the FORECAST function in Excel for principal component analysis (PCA). All available data (including  $\delta^{18}O_{paleo-precip}$ , Loss-on-Ignition (LOI) data sets from Stansell et al., 2017) with a currently updated age-depth scale),  $\delta^2 H_{n-alk}$  and chironomid results were analyzed using PCA with FactoMineR software in R (Husson et al., 2016). Insolation was modeled using Acycle package in Matlab (Li et al., 2019). The sequential Regime Shift Detection (Rodionov, 2004) software (v. 6.2) with a 95% confidence level and a Huber's tuning constant of 2 was used to detect shifts in  $\delta^{18}O_{calc}$  proxy record. All correlation coefficients presented are statistically significant (p  $\leq$  0.05).

Lake Päidre (11 km NW from Lake Nuudsaku) pollen profile (Saarse et al., 1995) age scale was updated with IntCAL20 (Reimer et al., 2020), and the species divided into gymnosperms, C3 mono- and dicots, bryophytes and pteridophytes. The pollen was also categorized as trees, herbs, shrubs and spores to assess the possible influence of vegetation shifts on the  $\delta^2 H_{n-alk}$ .

#### 4. Results

#### 4.1. Water isotopic compositions

The meteoric and lake surface water stable isotope composition in Estonia have been monitored since 2013. The  $\delta^{18}O_{precip}$  and  $\delta^{2}H_{precip}$ yield more negative values during cold season (November-April) than during warm season (May-October) due to isotopic fractionation caused by temperature changes (Dansgaard, 1964). Cold season (Nov-Apr)  $\delta^2 H_{precip}$  and  $\delta^{18} O_{precip}$  measured at the station are correlated with air temperatures and vapor pressure ( $\rho \geq 0.68$ ), but not precipitation amounts. Warm season (May–Oct)  $\delta^2 H_{precip}$  and  $\delta^{18} O_{precip}$  are slightly less correlated with air temperatures ( $\rho \geq 0.63$ ) and vapor pressure ( $\rho \geq$ 0.51) than during the cold season. Precipitation amounts are best characterized by vapor pressure ( $\rho = 0.47$ ) all year round. The instrumental (measured)  $\delta^{18}O_{precip}$  and  $\delta^{2}H_{precip}$  monthly (n = 66) median values correlate with the Piso.AI 2013 to 2018 (n = 66) modeled monthly median values ( $\rho = 0.94$  and  $\rho = 0.97$ , respectively) as well as with the 1900 to 2020 (n = 1440) Piso.AI data set ( $\rho$  = 0.92 and  $\rho$  = 0.94, respectively). The instrumental *d*-excess values lie between 2.90% and 14.24% (mean 8.25%, median 8.48%). The median of the monthly values of d-excess from Tartu-Toravere station were well correlated with the Piso.AI 1900 to 2020 *d*-excess data set ( $\rho = 0.64$ , p = 0.02).

The local evaporation line (LEL, y=4.97x-23.15) is defined by Estonian lake water isotope data (Fig. 3). The local meteoric water line (LMWL, y=7.61x+3.78) was calculated as a linear fit through the water isotope values (n=205) from this study (Supplemental Table 1), measurements by the GNIP station between 2013 and 2018, modeled Piso.AI data from 1901 to 2020, measured precipitation and surface water (wetlands, rivers, wells, springs) by Raidla et al. (2016), and by Stansell et al. (2017).

Cold season (Nov to April) precipitation has relatively lower values while warm season (May to Oct) water isotopes have higher values. Most of the lake water samples on Fig. 3 lie within the warm season isotopic range as these were collected during summer months. The lake water samples likely reflect a compounded precipitation water isotope signal

from at least a couple of months prior to each sampling date. The modern Nuudsaku lake water (n = 20)  $\delta^{18}$ O values range from -11.38% to -9.44% (mean -10.12%) and  $\delta^2$ H values between -80.9% and -69.5% (mean -73.2%). These samples were collected between April and December from 2014 to 2022 (Supplemental Table 1). Lake Nuudsaku modern water  $\delta^{18}$ O and  $\delta^2$ H values plot on the LMWL, indicating that the lake is not sensitive to evaporation (Fig. 3).

#### 4.2. Chronology

All lake Nuudsaku updated age-depth values and Bayesian model results are presented in Table 1 and Fig. 4. The sediment core overlaps were adjusted by a few centimeters, and there are four new radiocarbon ages in addition to the previously published seven  $^{14}\mathrm{C}$  ages (Stansell et al., 2017). The new age-depth model suggests the oldest mean calibrated age of  $\sim\!10$  070 cal yrs BP, and the oldest modeled age of  $\sim\!9990$  cal yrs BP.

#### 4.3. Loss-on-Ignition

A total of 172 LOI measurements from the Lake Nuudsaku core are presented with an updated age-depth scale on the Supplemental Fig. 1. The % organic matter (OM; LOI @ 550 °C), carbonate (LOI @ 1000 °C) fraction abundances are reproduced from Stansell et al. (2017). The middle Holocene OM averaged at 37  $\pm$  7%, and the late Holocene value at 22  $\pm$  10% (1 $\sigma$ ). Carbonate content in lake Nuudsaku was 21  $\pm$  10% during the middle, and 14  $\pm$  5% (1 $\sigma$ ) during the late Holocene.

#### 4.4. Chironomid analyses and July temperature reconstruction

There were 45 Chironomid taxa found in the Lake Nuudsaku sediment profile with a total of 2027 head capsules counted (n = 39) The CI-TJul values ranged from 15.0 °C to 20.3 °C (mean 17.7 °C) with the highest temperature recorded at 7300 cal yrs BP and the lowest at  $\sim$ 1400 cal yrs BP (Supplemental Fig. 2). The middle and late Holocene Ci-TJul averages did not notably differ (>0.5 °C). This temperature variability reflects changes in the Chironomid abundances, which also contribute to the PCA scores. The chironomid PCA axis 1 (including only the most common species) explained 13.9 % and axis 2 explained 12.5 % of the entire variance. Chironomus plumosus-type ( $\rho = 0.58$ ) and Cricotopus (I.) intersectus-type ( $\rho = 0.50$ ) species contributed the most to PCA axis 1. The most contributing species to PCA axis 2 were Glyptotendipes pallens-type ( $\rho = 0.72$ ) and Limnophyes ( $\rho = 0.69$ ). Procladius species occurred in all samples. Chaoborus flavicans are abundant in deep as well as shallow eutrophic lakes (Luoto and Nevalainen, 2009), and the relative content of this species in Lake Nuudsaku record was relatively high, making up > 45% of all head capsules counted between ~5800 and  $\sim$ 5200 and at  $\sim$ 2800 cal yrs BP.

#### 4.5. Carbon and nitrogen isotopes and elemental abundance

Three out of the 13 total samples selected for carbon and nitrogen analyses were from middle Holocene sediments and the rest from the late Holocene. The TOC in Lake Nuudsaku sediments varied between 4.3% and 18.2% with the lowest value recorded at the bottom of the record at ~7500 cal yrs BP and the highest at ~2800 cal yrs BP. The TN changed in a respective manner from 0.4% to 1.3% (Supplemental Fig. 3). The calculated C/N values (weighted mean) averaged at 15.8 from ~7500 to ~1500 cal yrs BP and at 13.3 from ~1200 to ~400 cal yrs BP,  $\delta^{15}$ N at 1.4% and 3.2% (vs AIR), respectively. Carbon stable isotope values from bulk sediment ( $\delta^{13}C_{bulk}$ ) ranged from ~28.2% to ~18.1% (25.3% mean, vs VPDB) and  $\delta^{13}C$  from organic matter ( $\delta^{13}C_{org}$ ) between ~38.0% and ~31.3% (~33.3% mean). The TN and TOC were significantly correlated with each other ( $\rho$  = 0.95) indicating no preferential degradation of these proxy data (Meckler et al., 2004). The TOC and TN were in positive correlation with  $\delta^{13}C_{bulk}$  ( $\rho$   $\geq$  0.90) and in

Table 1

Lake Nuudsaku radiocarbon (14C) and 210Pb ages used in the current study. New radiocarbon dates are marked by asterisks (\*) after the sample lab number in the first column, all other ages presented are from Stansell et al. (2017). Radiocarbon ages were calibrated using IntCal20 (Reimer et al., 2020), using the R package BACON (Blaauw and Christen, 2018). Minimum and maximum calibrated and modeled ages (years before 1950 CE) represent the 95% range.

UCI <sup>14</sup> C Lab #	Material	Depth (cm)	Measured <sup>210</sup> Pb/ <sup>14</sup> C age	Measured error $(\pm)$	Calibrated ages			BACON modeled ages		
					min	median	max	min	mean	max
	<sup>210</sup> Pb sample	0.375	-51	6.7				-71	-60	-35
	<sup>210</sup> Pb sample	0.875	-35	7.6				-70	-57	-30
	<sup>210</sup> Pb sample	1.375	-8	4.3				-70	-54	-22
218706*	Plant macro	55.55	1010	60	652	930	1208	51	459	878
146782	Charcoal	155.7	735	50	501	684	883	612	878	1296
146783	Charcoal	231.7	1600	90	1167	1528	1884	1344	1586	1926
218707*	Leaf fragment	271.7	2345	35	2110	2418	2730	2155	2347	2602
218708*	Leaf fragment	434.5	3795	20	3973	4195	4417	4015	4167	4287
146785	Charcoal	458.3	3180	100	2864	3380	3896	4155	4391	4758
146786	Charcoal	550.6	5145	20	5730	5874	6018	5758	5891	5989
146787	Charcoal	617.1	6070	50	6631	6934	7237	6713	6904	7136
146788	Charcoal	685.2	6480	160	6665	7315	7965	7322	7689	8292
218709*	Leaf fragment	700	7490	300	7292	8453	9613	7724	8363	9145
146789	Birch leaf	729	8960	25	9876	10068	10260	9653	9986	10196

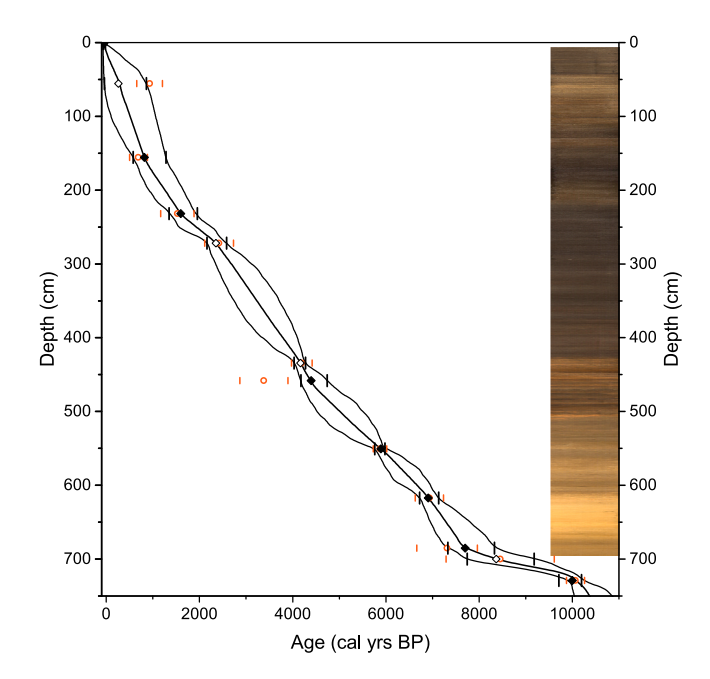


**Fig. 4.** Lake Nuudsaku age-depth model with a sediment image profile on the right. Black diamonds and the middle line represent modeled BACON mean age values at given depths. Open diamonds denote new radiocarbon ages. The vertical error bars and the outer lines represent the age model uncertainty range. Original calibrated median values are shown as orange empty circles, and the accompanying error range as orange vertical bars.

negative correlation with  $\delta^{13}C_{org}$  ( $\rho \leq -0.95$ ).

# 4.6. Sedimentary n-alkane distribution

Leaf wax n-alkanes were found in all Lake Nuudsaku samples (n = 30), and the distributions were dominated by odd numbered compounds. The most abundant n-alkanes in the sediment record were n- $C_{27}$  and n- $C_{29}$  with 7.6 and 8.3 µg/g content averages, respectively (Fig. 5). The sum of all even and odd numbered n-alkanes (n- $C_{17}$ - $C_{35}$ ) ranged from 13.5 to 86.5 µg/g per sample. The middle Holocene average content of all n-alkanes (n- $C_{17}$ - $C_{35}$ ) was 26.8 µg/g per dry sediment sample and the late Holocene average roughly doubled that at 50.7 µg/g per sample. The relative contribution of n-alkanes changed throughout the record (Fig. 5). The n- $C_{19}$  curve was the most variable changing from 0.3 to 20.5% (1 $\sigma$  = 5.6), and n- $C_{33}$  the least variable with relative

abundances between 2.0 and 5.2% ( $1\sigma=0.8$ ). The n-C $_{29}$  and n-C $_{27}$  had the highest mean relative abundance values of 26.2 and 23.6%, respectively.

Positive correlations of the odd-chain n-alkanes (n-C<sub>17-35</sub>) were found between n-C<sub>23</sub> and n-C<sub>25</sub> ( $\rho=0.62$ ), n-C<sub>29</sub> and n-C<sub>31</sub> ( $\rho=0.81$ ), n-C<sub>31</sub> and n-C<sub>33</sub> ( $\rho=0.66$ ) contents, and negative between n-C<sub>23</sub> and n-C<sub>29-33</sub> ( $\rho<-0.49$ ) as shown in Supplemental Table 2. The relative proportion of n-C<sub>33</sub>/n-C<sub>31</sub> (not shown) describing the abundance of grasses (Colcord et al., 2018) in Lake Nuudsaku sediments was the highest (-2.5 average) between 8400 and 4200 cal yrs BP, then decreased to -5.9 until 3000 cal yrs BP, whereafter rising to an average of -3.5 until the modern time.

Average chain length (ACL) values varied from 26.8 to 28.3 throughout the core. The ACL weighted average was 27.3 from  $\sim\!\!8400$  to  $\sim\!\!6000$  cal yrs BP, which increased to 28.2 from thereafter until  $\sim\!\!4200$  cal yrs BP, and then decreased to 27.8, remaining at this level until modern time. The carbon preference index (CPI) in the sediments was between 2.0 and 10.0 with weighted average values of 4.9 from  $\sim\!\!8400$  to 3200 cal yrs BP, followed by higher values (8.4) until the modern time. There was no correlation between the ACL and CPI. The ACL was negatively but well correlated with  $P_{aq}$  ( $\rho=-0.99$ ). The  $P_{aq}$  (Fig. 5) results varied from 0.23 to 0.55 (median 0.39) with relatively decreased values ( $\sim\!\!0.25$ ) between  $\sim\!5700$  and  $\sim\!\!4500$  cal yrs BP.

# 4.7. $\delta^2 H_{n-alk}$ , relative humidity, $\delta^{18}O$ and d-excess

The  $\delta^2 H_{n\text{-alk}}$  values in Lake Nuudsaku sediment samples (n = 30) varied between -201% and -137% with the greatest variability (1 $\sigma$ ) occurring in  $\delta^2 H_{C23}$  (21%),  $\delta^2 H_{C31}$  (19%) and  $\delta^2 H_{C25}$  (16%), and slightly less variability in the  $\delta^2 H_{C29}$  (13%) and  $\delta^2 H_{C27}$  (9%) data sets (Fig. 6). The individual  $\delta^2 H_{n\text{-alk}}$  profiles show significant correlation with each other ( $\rho \geq 0.69$ ). Correlation is the highest between  $\delta^2 H_{C23}$  and  $\delta^2 H_{C25}$  ( $\rho = 0.96$ ), and between  $\delta^2 H_{C29}$  and  $\delta^2 H_{C31}$  ( $\rho = 0.94$ ), indicating that these compounds likely have similar sources. The  $\delta^2 H_{C23}$  values ranged between -206% and -137%, and the  $\delta^2 H_{paleo-precip}$  between -123% and -47%. The non-weighted average fractionation between terrestrial and aquatic  $\delta^2 H$  ( $\epsilon_{2\text{Hterr/aq}}$ ) varied between -49.1% and 23.8% (Fig. 6), with the modern value at -18.3%. The calculated Monte Carlo range for our  $\epsilon_{2\text{Hterr/aq}}$  was at an average of 0.05%.

The reconstructed  $\Delta RH$  (smoothed) values at Lake Nuudsaku varied between -12% and 11% in comparison to modern (Fig. 6). The lowest value occurred at 3000 cal yrs BP, and the highest at 6600 cal yrs BP. The average middle Holocene  $\Delta RH$  value is 1%, and the late Holocene value -5% in comparison to modern. The average  $\Delta RH$  model error was 3%.

Stansell et al. (2017) demonstrated that the Lake Nuudsaku surface sediment  $\delta^{18}O_{calc}$  value was -12.5% (vs VPDB). We calculated the

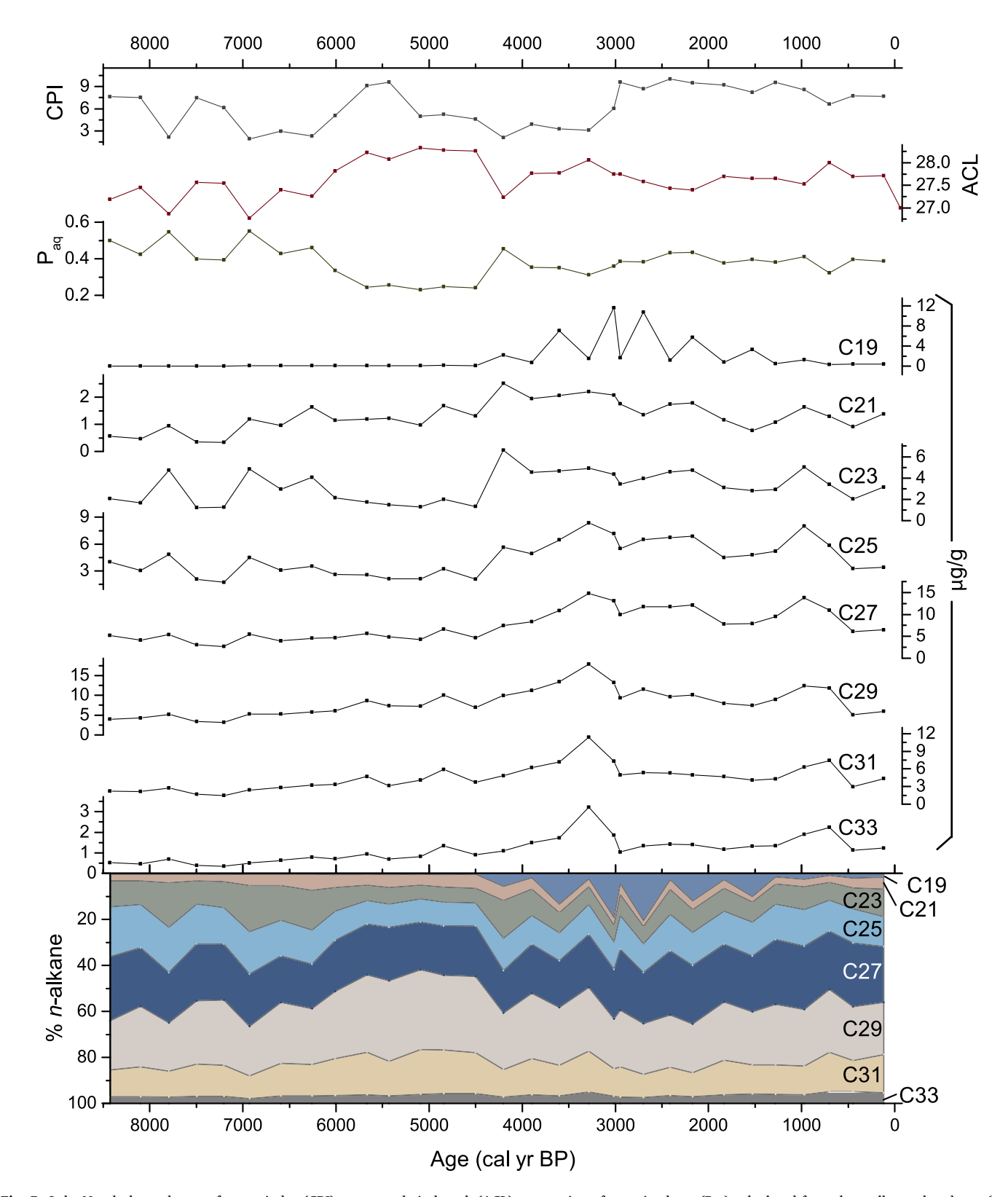


Fig. 5. Lake Nuudsaku carbon preference index (CPI), average chain length (ACL), proportion of aquatic plants ( $P_{aq}$ ) calculated from the n-alkane abundance (see methods for details), n-alkane content (from n- $C_{19}$  to n- $C_{33}$ ) and relative abundances (bottom colored plot).

 $\delta^{18}O_{paleo\text{-precip}}$  value of -11.6% (vs VSMOW) from the same  $\delta^{18}O_{calc}$  (after Kim et al., 2015), which is in an agreement with the modern  $\delta^{18}O_{precip}$  range (mean -11.00% vs VSMOW). The  $\delta^{18}O_{calc}$  values from the same lake sediments (Stansell et al., 2017) ranged from -15.0% to -9.4% (vs VPDB) that translates (Leng and Marshall, 2004) to values

between 15.4% and 21.3% (vs VSMOW). Our calculated  $\delta^{18}O_{paleo \cdot precip}$  values lie between -11.6% and -9.2% (vs VSMOW), with the average middle Holocene value of -10.2% and late Holocene value of -10.5%.

The calculated unsmoothed d-excess values ranged from -40.4% to 35.8% throughout the Lake Nuudsaku sediment profile (Fig. 6), and the

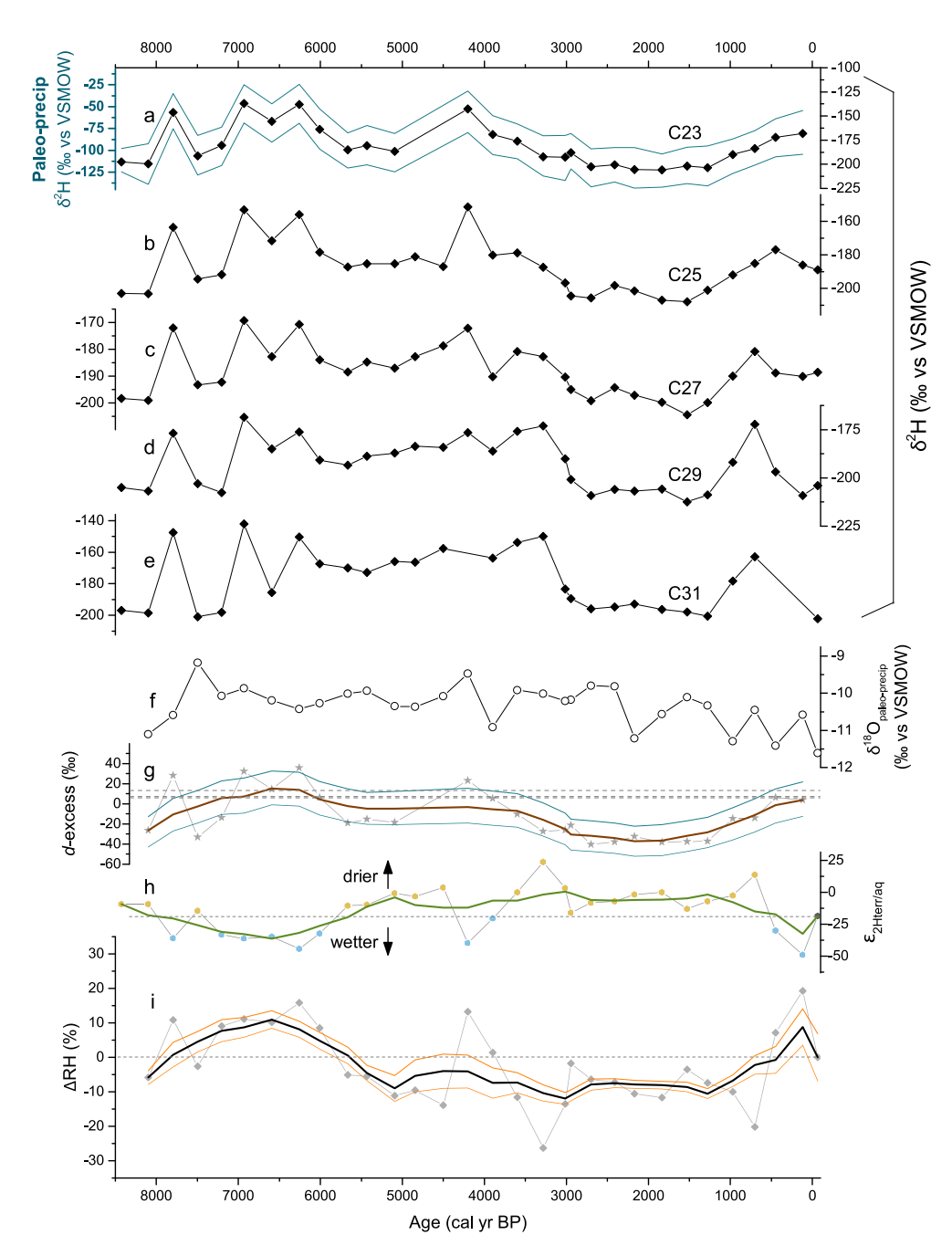


Fig. 6. Lake Nuudsaku sediment-derived  $\delta^2H$  values of odd-chain n-alkanes ( $\delta^2H_{C23-31}$ ; a to e);  $\delta^2H_{paleo-precip}$  (a);  $\delta^{18}O_{paleo-precip}$  (f); d-excess calculated from  $\delta^2H_{paleo-precip}$  and  $\delta^{18}O_{paleo-precip}$  (g); fractionation between terrestrial (n-C<sub>29</sub>) and aquatic (n-C<sub>23</sub>) n-alkane derived  $\delta^2H$  (ε<sub>2Hterr/aq</sub>; h); and ΔRH = relative humidity (calculated from ε<sub>2Hterr/aq</sub>; i). The d-excess plot (g) shows calculated values as stars, which is overlain by a smoothed bold brown line (points of window = 5). Gray dashed lines on the d-excess plot (g) mark the Piso.AI modeled mean values from 1900 to 2020 (7.7‰), modern GNIP mean d-excess from 2013 to 2018 (8.3‰) and the reconstructed mean surface sediment (13.2‰) value. The gray dashed line on the ε<sub>2Hterr/aq</sub> plot (h) marks the modern value, and the green bold line represents smoothed adjacent-averages (points of window = 5). Monte Carlo ranges are marked by blue lines in panels a and g. Change in the relative humidity (ΔRH; i) values are normalized to 81.3%, an average RH from 5 years prior to surface sediment extraction 2010–2014, and shown as relative to the modern value (dashed line). The gray ΔRH data as symbols represent model output (following Rach et al., 2017), which is overlain by an adjacent-averaging smoothed bold black line (points of window = 5), and orange lines represent smoothed model error ranges. Modern surface sediment  $\delta^2H_{C25.31}$  values were acquired from Eensalu et al. (2023).

smoothed values between -37.1% and 15.1%. The middle Holocene average value was -1%, and the late Holocene average was -19%. The reconstructed d-excess value of the surface-most sediment sample from 120 cal yrs BP (3.7%) falls within the  $1\sigma$  error range of the modern GNIP data from 2013 to 2018 between 2.9 and 14.2% (mean 8.3%) and the Piso.AI modeled values from 1900 to 2020 that were between -8.4 and 24.2% (mean 7.7%; Fig. 6).

# 5. Discussion

# 5.1. Evidence from $\delta^{15}N$ , $\delta^{13}C$ and loss-on-ignition data

Bulk sediment organic matter  $\delta^{15}N$  and  $\delta^{13}C$  values have been used for reconstructing lake hydrological and ecological evolution (Brenner et al., 1999; Meyers and Teranes, 2001), however these proxies greatly depend on the local ecological and hydrological parameters, and can be

highly variable due to catchment topography, basin morphology, lake internal processes (such as nutrient loading, water and sediment mixing), surrounding vegetation, human impact and climate change (Meyers and Lallier-Vergès, 1999; Herzschuh et al., 2005). The relatively lower  $\delta^{15}\mbox{N}$  values (1.4‰) in the Lake Nuudsaku proxy from the base of the record at  $\sim 7500$  cal yrs BP until  $\sim 1200$  cal yrs BP likely reflect lower lake primary productivity (Supplemental Fig. 3) as nitrogen is a key limiting nutrient in lakes (Altabet and François, 1994). Increased values (3.2%) towards the top of the record after  $\sim 1200$  cal yrs BP possibly point to slightly higher productivity, which was likely a result of several changing ecological and/or climate parameters at Nuudsaku. The four-fold increase in TOC values (4.3–18.2%) from  $\sim$ 7500 to  $\sim$ 2800 cal yrs BP roughly tracks the sediment organic matter (LOI @ 550 °C) curve and probably suggests increased allochthonous matter input to the lake and/or increased vegetation presence near the lake. Despite the increasing TOC, the C/N ratios are fairly constant (ranging between 13.2 and 16.9) throughout the entire record, indicating that the partitioning between terrestrial and aquatic sources remained stable. Interestingly, Lake Nuudsaku data show a similar decrease in C/N to Lake Trikātas after ~1500 cal yrs BP, which the authors attributed to an increased input of algal matter related to increased soil erosion due to anthropogenic land use (Stivrins et al., 2019). The  $\delta^{13}C_{\text{bulk}}$  values (-18.1%) at the base of the sediment core at  $\sim 7500$  cal yrs BP suggest high carbonate matter proportion in the lake which is also supported by relatively high endogenic calcite content (LOI @ 1000 °C = 27.9%; Supplemental Fig. 1).

#### 5.2. Potential sedimentary n-alkane sources

The Lake Päidre pollen profile (Saarse et al., 1995) consisted of 50 samples between ~ 9000 and 1250 cal yrs BP (Supplemental Fig. 5). The abundance of tree pollen ranged from 85.1% to 93.0% (mean 89.6%) throughout the Lake Päidre core while herbs made up 3.9% to 9.2%, shrubs 0.6% to 4.1% and spores 1.3% to 4.9%. The most abundant species in this record were *Alnus*, *Betula*, *Picea and Pinus*. The correlation between trees versus other groups was negative throughout the record. Relative overall abundance of C3 dicot pollen counts in the Lake Päidre record was 62% while gymnosperms made up 29%. The rest of the 9% plant types were C3 monocots and dicots, Bryophytes and Pteridophytes.

Modern plant odd-chain n-alkane composition at Lake Nuudsaku (Eensalu et al., 2023) shows high abundance (>43  $\mu$ g/g) of n-C<sub>31</sub>, n-C<sub>29</sub> and n-C<sub>27</sub> alkanes, and relatively low (~4 μg/g) n-C<sub>23</sub> content (Supplemental Fig. 4). Other studies have reported similar distributions of angiosperm plants (Diefendorf et al., 2011; Bush and McInerney, 2013). Based on the abundance of the Lake Nuudsaku sedimentary n-alkane and Lake Päidre pollen data, we find that the sedimentary n-C<sub>23</sub> is positively well correlated with Corylus ( $\rho=0.52$ ), Alnus ( $\rho=0.51$ ) and Ulmus ( $\rho$ = 0.48), and negatively with Picea ( $\rho$  = -0.54) and aquatic Nymphaeaceae ( $\rho = -0.36$ ). However, the lack of high correlation between abundances of n-C23-25 and n-C27-31 in the Nuudsaku sediments (Supplemental Table 2) suggests that each of these groups have a common source, but these two sources are different from each other. The simultaneous lack of correlation between n-C23-25 and n-C27-31 abundances, and positive correlation between n-C23-25 and tree species pollen from Lake Päidre is difficult to explain, but may represent an indirect lake productivity signal in response to temperature changes as deciduous trees prefer warmer climates, and coniferous species thrive in colder conditions (Poska et al., 2004). There is a negative correlation between Lake Nuudsaku n- $C_{23}$  alkane and Lake Päidre aquatic pollen profile (Supplemental Table 2). Therefore, the marsh-type emergent plant groups are likely not the major sources of n-C23 and n-C25, but we emphasize that the pollen record represents another lake basin. While the pollen record from terrestrial species is likely easily transferred between nearby lake basins, data from aquatic plants would only be expected to apply if external factors drove similar expansion or contraction

in both lakes. This necessarily increases the uncertainty for interpreting aquatic pollen sources at Lake Nuudsaku based on the Lake Päidre pollen data.

The decreasing C3 dicot composition during the middle Holocene (Supplemental Fig. 5) is likely reflected in the Lake Nuudsaku  $\delta^{13}C_{org}$  record (Supplemental Fig. 3). We suggest this as gymnosperms and C3 dicots make up most (91%) of the components in the nearby Lake Päidre pollen record, and the relative proportion of C3 dicots (primarily deciduous plants) in Lake Päidre decreases from  $\sim\!9000$  to  $\sim\!2800$  cal yrs BP while gymnosperm (coniferous tree) pollen increases (Supplemental Fig. 5). Therefore, this change in vegetation most likely explains the 7% gradual increase in lake Nuudsaku  $\delta^{13}C_{org}$  values from the start of the record until  $\sim\!2800$  cal yrs BP.

The Päidre pollen PCA dimension 1 likely reflects the relative change of gymnosperms and C3 dicots (Supplemental Fig. 5). However, the relative proportion of trees versus shrubs, herbs and spores in Lake Päidre pollen record does not notably change over the course of the last 9000 years (Supplemental Fig. 5). The weighted average  $\delta^2$ H value of plant groups in Lake Päidre pollen profile resulted in a negligible 3.2‰ difference across all counts. Although small, we did incorporate Lake Päidre pollen correction (Feakins, 2013; Rach et al., 2017) to Lake Nuudsaku  $\delta^2$ H<sub>n-alk</sub> data for reconstructing past  $\Delta$ RH values.

The relatively low C/N values during the late Holocene (<17; Supplemental Fig. 3) likely indicate that the n-alkane source is at least partially of aquatic origin at that time. The Pag is generally an indicator of the relative dominance of terrestrial (<0.1) versus aquatic (>0.4) taxa, although most of the values in Lake Nuudsaku lie within the range of 0.2 to 0.4, which Ficken et al. (2000) classify as emergent (Fig. 5). The period between ~6000 and ~4500 cal yrs BP showed decreased n-C<sub>23</sub> and n-C<sub>25</sub> and increased n-C<sub>27</sub>, n-C<sub>29</sub> and n-C<sub>31</sub> content in comparison to the earlier middle Holocene, which is also reflected in the ACL profile. Aichner et al. (2017) demonstrated that lipid distributions can exhibit significant variability, with many aquatic plants lacking alkanes shorter than n-C<sub>23</sub>. The absence of shorter alkanes therefore does not negate the possibility of an aquatic source dominating the lipid composition. While the use of alkanes is limited due to their lack of perfect source specificity, there are overarching patterns that can still offer valuable insights into the lake catchment. For example, our results (Fig. 5) reveal the presence of n-C<sub>19</sub> and n-C<sub>33</sub> alkanes, but we were analytically limited to determining the  $\delta^2$ H values in the n-C<sub>23</sub> and n-C<sub>31</sub> range.

The biomarker composition in Lake Nuudsaku has a high odd-overeven and dominantly long-chain n-alkane distribution, and the median CPI value of 7.4 implies that the *n*-alkane sources at the lake are primarily terrestrial leaf waxes with very little compound degradation (Bush and McInerney, 2013). The relatively higher ACL (27.8) in Lake Nuudsaku sediments between ~ 6900 and ~4500 cal yrs BP may suggest increasing aridity (Keisling et al., 2017), most likely as a result of relatively high, yet declining warm season insolation (Fig. 7). Our  $\Delta RH$  and  $\epsilon_{2Hterr/ag}$  proxies (Fig. 7) are in an agreement with this interpretation as these indicate that the moisture content at Lake Nuudsaku decreased during that time interval. Furthermore, the ACL, CPI and n-alkane contents were lower at ~7800 cal yrs BP in comparison to the rest of the record. This could be explained by soil stabilization due to increased vegetation in the lake catchment (Operstein and Frydman, 2000). There is a period from ~3000 to ~2000 cal yrs BP where CPI values are high (>9.5) while ACL is relatively low (<27.7) due to the occurrence of high n-C<sub>17</sub> content of algal origin, which may be linked to changes in land use.

# 5.3. Sedimentary $\delta^2 H$

The sedimentary  $\delta^2 H_{n\text{-}alk}$  record at Lake Nuudsaku most likely incorporates the  $\delta^2 H_{paleo\text{-}precip}$  signal as the modern terrestrial plant  $\delta^2 H_{n\text{-}alk}$  values reflect  $\delta^2 H_{precip}$  signal during the leaf flush period from May to June (Eensalu et al., 2023). The same study suggested that the  $\delta^2 H_{precip}$  value of n-alkanes reflects a compounded  $\delta^2 H_{precip}$  signal from at least a few months prior to sampling, until the end of leaf flush period.

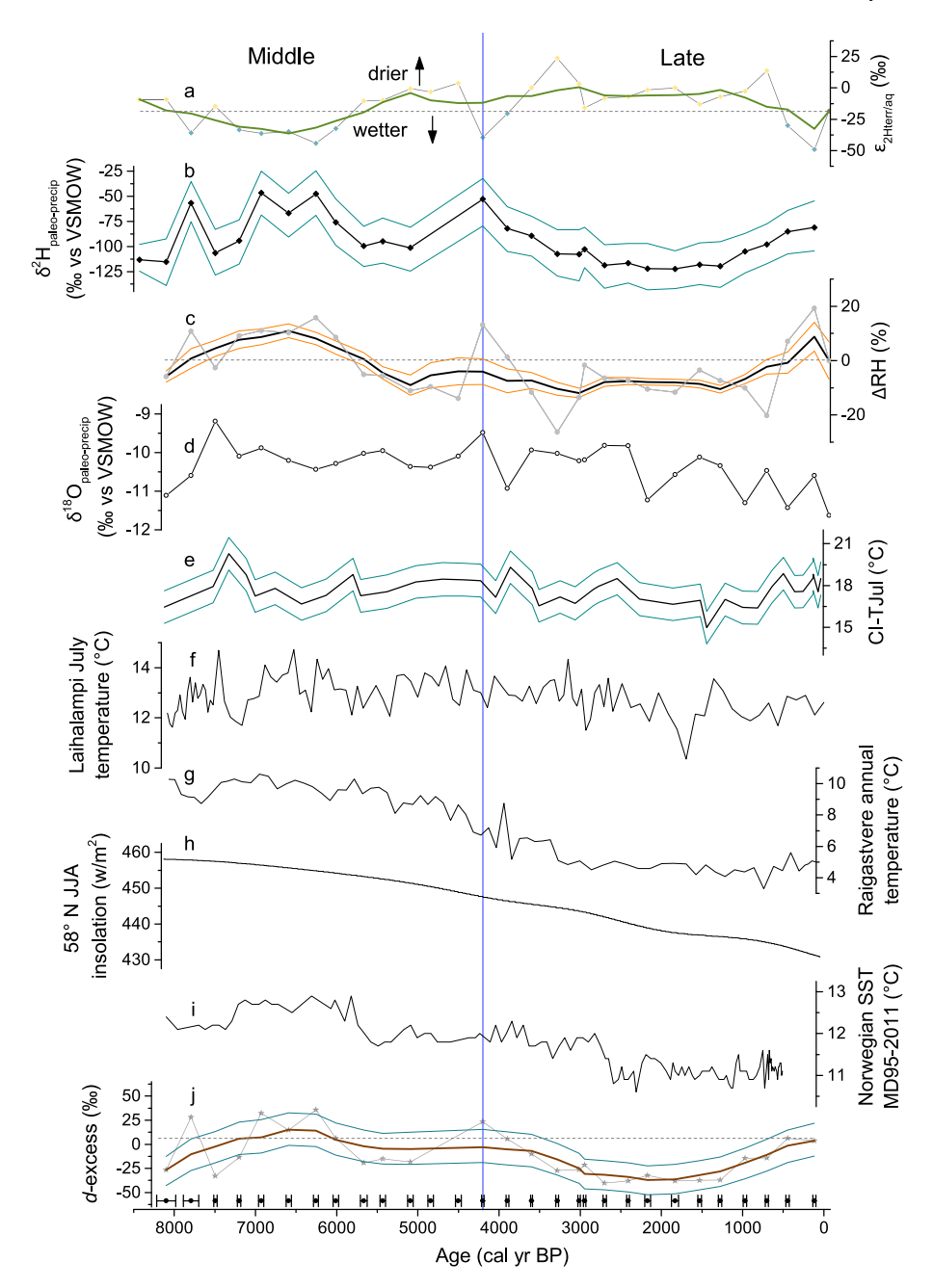


Fig. 7. From top to bottom: Lake Nuudsaku  $\varepsilon_{2Hterr/aq}$  representing wet vs dry conditions (a) shown as a gray line with wet conditions marked as blue and dry conditions as yellow symbols, overlain by an adjacent-averaging smoothed bold green line (points of window = 5);  $\delta^2 H_{paleo-precip}$  (reconstructed from  $\delta^2 H_{C23}$ ; b); relative humidity change ( $\Delta$ RH) modeled after Rach et al. (2017) shown as a gray symbols and line, overlain by a 5-pt smoothed black line, and the orange lines represent smoothed model error ranges (c); Lake Nuudsaku temperature  $\delta^{18}O_{paleo-precip}$  (d) and chironomid-inferred July temperatures (CI-TJul; e); July temperature reconstruction from Laihalampi, Finland (f; Giesecke et al., 2008); annual temperature reconstruction from Raigastvere, Estonia (g; Seppä and Poska, 2004); modeled warm season (JJA) insolation at 58 °N (h; using R package Acycle); Norwegian alkenone-based SST reconstruction (i; Grimalt and Marchal, 2006); Lake Nuudsaku *d*-excess representing moisture origin (j) as a gray line with symbols, and bold brown show a 5-pt smoothed data of the *d*-excess with blue lines as smoothed Monte Carlo ranges. Blue lines in panels b and e represent non-smoothed Monte Carlo ranges. The symbols with bars above the *x*-axis at the bottom of the figure mark sample ages and 95% uncertainty ranges. The vertical line across all panels separates the middle and late Holocene periods at 4200 cal yrs BP. Gray horizontal dashed lines mark modern values.

The calculated  $\delta^2 H_{paleo-precip}$  from our topmost sediment ( $\sim$ -81  $\pm$  4‰; Monte Carlo range  $\pm$  25‰) at Lake Nuudsaku is in the range of both modern instrumental and modeled  $\delta^2 H_{precip}$  values ( $\sim$ -80‰; Figs. 2 and 6). There was a gradual change from -51% to -122% in the  $\delta^2 H_{paleo-precip}$  from 4200 to 2500 cal yrs BP, which may have been a result of prevailing colder summer temperatures (decreasing CI-TJul values), warmer source water temperatures (decreasing *d*-excess; Fig. 7), or a combination of these two. These changes could not be

explained by an increase in cold season precipitation because our  $\epsilon_{2Hterr/aq}$  demonstrates relatively drier conditions at that time. According to Sachse et al. (2012), the median  $\epsilon_{app}$  values (calculated between  $\delta^2H$  of mean annual precipitation and  $\delta^2H_{C29})$  of gymnosperms and C3 dicots are -110% and -118%, respectively. The two dominant taxonomic categories in the Lake Päidre record range between 10% and 51% (gymnosperms), and 40%–81% (C3 dicots). Leaving the rest of the taxa of 9  $\pm$  3% (2 $\sigma$  range) aside, the lowest

gymnosperm and highest dicot assemblage results in a -107% average, and the opposite in a -105% average, which would only explain a  $\sim\!2\%$  shift in the  $\delta^2H_{paleo-precip}$  values. According to the GNIP data from 2013 to 2018 at the Tartu Tōravere station, a 1 °C increase would correspond to a  $\sim\!4\%$  increase in  $\delta^2H_{precip}$  (T (°C) =  $\delta^2H_{precip}\times0.2527+26.813;~\rho=0.56$ ). However, as our reconstructed CI-TJul varies between 16.5 °C and 19.3 °C, the CI-TJul temperature shift of 5.3 °C is highly unlikely, but would theoretically result in  $\sim\!21\%$  change in  $\delta^2H_{paleo-precip}$ . There is a strong correlation between modern  $\delta^2H_{precip}$  (and  $\delta^{18}O_{precip}$ ) and air temperature at Lake Nuudsaku ( $\rho=0.69;~Fig.~2$ ), characteristic of higher latitudes (Dansgaard, 1964). Therefore, the decrease to lower values between 4200 and 2500 cal yrs BP is most probably a combination of lower warm season temperatures at Nuudsaku, and higher source water temperatures (decreasing d-excess).

# 5.4. Hydroclimate signals inferred from d-excess, $\Delta RH$ and $\varepsilon_{2Hterr/aq}$

The *d*-excess value of vapor evaporating from water varies due to the effects of temperature and relative humidity on the degree of kinetic isotope fractionation. These effects can be broadly characterized by a 0.35% increase per  $^{\circ}$ C and a -0.43% decrease per % relative humidity for evaporation above the ocean, which is the primary source for precipitation (Feng et al., 2009). Additional *d*-excess signals in precipitation can also indicate evaporation of water from a non-ocean source, either as re-evaporated precipitation or evaporation from inland water bodies, soil water, or plant transpiration (Aemisegger et al., 2014). Precipitation in northern Europe tends to originate from the North Atlantic during cold seasons, while modern warm season precipitation in Estonia originates from both the Atlantic ocean as well as the Mediterranean and the Black Sea area (Mätlik and Post, 2008). These moisture sources should therefore carry distinct d-excess signals which can be used to distinguish changes in precipitation sources or seasonality through time (Xia et al., 2022).

The hydroclimate in northern Europe is affected by moisture source changes (Pfahl and Sodemann, 2014; Stansell et al., 2017; Kopec et al., 2019). The short-term *d*-excess in the individual marine regions generally shows low summer and high winter values (Aemisegger et al., 2014; Kopec et al., 2019). On a seasonal scale, Klein et al. (2015) associate higher *d*-excess in Arctic Alaska with northerly sources and lower humidity at the source, which is also consistent with other work showing that northern sources have higher *d*-excess precipitation values (Puntsag et al., 2016). Additionally, a recent European study indicates that precipitation during storms from a northern source, Barents Sea, resulted in relatively higher *d*-excess values (Bailey et al., 2021).

Similarly, we suggest that the long-term change in moisture source arriving at Nuudsaku could result in higher d-excess from northern, and lower d-excess from the southern moisture sources. A recent study, which could serve as a modern analog, recorded higher d-excess values during higher winter precipitation events with northern sources (Puntsag et al., 2016). However, long-term d-excess records in the mid-latitude regions are scarce, and it is possible that the annual means may mask the inferred seasonal changes (Aemisegger et al., 2014).

The Lake Nuudsaku mean d-excess value of  $1.6 \pm 5\%$  (MC  $\pm 17\%$ ) between 8100 and 3900 cal yrs BP is in the range of the modern value (Fig. 3) inferred from the surface lake sediments (3.7  $\pm$  4‰), the instrumental (8.3  $\pm$  3‰) data, and the global value of 6.85  $\pm$  6.2‰ (Putman et al., 2019). Our data suggests that the precipitation reaching lake Nuudsaku between  $\sim$ 8100 and  $\sim$ 3900 cal yrs BP was similar to that of today, and generally originated more from northern areas in comparison to the subsequent millennia. However, the late Holocene average value of -19% is significantly lower than the mean annual values recorded in the northern high latitude regions ( $\sim$ 0‰ in Svalbard, according to Mellat et al. (2021) measurements conducted in the summer of 2018). This discrepancy could be attributed to noise, a temporal mismatch between the water isotope formation, variability in the mean

ecosystem apparent fractionation, changes in moisture sources, or a combination of these factors. We therefore focus on the broad trends and patterns in the reconstruction, acknowledging the potential for uncharacterized uncertainty in the reconstructed values.

Our  $\Delta RH$  reconstruction suggests that the period between 8100 and 6000 cal yrs BP was relatively wet (mean 7%) in comparison to modern (defined as 0% which is equivalent to the mean annual RH of 81%). There was a shift in seasonality after 6000 cal yrs BP, and the reconstruction suggests that  $\Delta RH$  values between 5800 and 700 cal yrs BP were  $\sim$ 8% lower than modern, and  $\sim$ 13% higher thereafter. Similarly, the  $\epsilon_{2Hterr/aq}$  in the Lake Nuudsaku record indicates that the period between 8100 and 5800 cal yrs BP was likely wetter than today, more arid between 5700 and 700 cal yrs BP, and again wetter thereafter until reaching the modern values.

#### 6. Holocene paleoclimate

#### 6.1. End of the early Holocene

The beginning of our  $\delta^2 H_{n-alk}$  record is dated at 8500 cal years BP, before the start of the middle Holocene (8200 cal years BP). From this early to middle Holocene transition, we highlight the most <sup>2</sup>H-depleted  $\delta^2 H_{aq}$  (~-200%) and  $\delta^2 H_{paleo-precip}$  (~-115%) values at the base of the record (from 8500 to 8100 cal years BP), which may reflect increased winter precipitation. The so-called 8.2 ka cold event (Walker et al., 2012) falls within that time range. However, Lake Nuudsaku ΔRH and  $\varepsilon_{2Hterr/ag}$  records suggest that this cold event in Estonia was slightly drier in comparison to the following millennia. The 8.2 ka event therefore likely exhibited similar conditions to modern day negative phase of NAO, or positive phase of SCP, which are characterized by cold and dry conditions. An Estonian study has documented this event by observing a significant decrease in their  $\delta^{18}O_{calc}$  record in annually layered Lake Rõuge Tõugjärv sediments (ca 100 km SE from Lake Nuudsaku), which translates to a  $\sim$ 3 °C decrease in annual temperatures between 8200 and 8080 cal yrs BP (Veski et al., 2004). This temperature anomaly is also recorded in Lake Laihalampi summer temperature reconstruction (Giesecke et al., 2008, Fig. 7). The  $\delta^2 H_{precip}$  and  $\delta^{18} O_{precip}$  are directly related to mean annual temperature (Dansgaard, 1964), as cold season precipitation has lower isotope values, and the opposite can be observed for warm season precipitation (Figs. 2 and 3) at Lake Nuudsaku.

#### 6.2. The middle Holocene

Higher  $\delta^2 H_{paleo-precip}$  (-85  $\pm$  25‰, 1 $\sigma$ ),  $\delta^{18} O_{paleo-precip}$  (-10.2  $\pm$ 0.4‰) and  $\epsilon_{2Hterr/aq}$  ( $-19.3\pm16$ ‰) values during the middle Holocene (between 8200 and 4200 cal yrs BP) at Lake Nuudsaku suggest increased summer precipitation in comparison to the late Holocene (Fig. 7). A recent study (Corcoran et al., 2021) suggested that higher  $\delta^2 H_{n-alk}$  values could be a result of increased evaporation from the lake surface, which in turn would result in slower lake water turnover times. However, lake Nuudsaku modern isotope data do not suggest any evaporation signals as the modern lake water samples plot on the LMWL (Fig. 3). Cold season hydrological conditions did not therefore likely have a significant impact on the  $\delta^2 H_{n-alk}$ , even though there may not have been ice cover on the lakes during the middle Holocene. Besides, the  $\epsilon_{2Hterr/aq}$  suggests relatively wetter conditions until 5800 cal yrs BP (Fig. 7). Thus, we interpret the higher  $\delta^2 H_{paleo-precip}$  and  $\delta^{18} O_{paleo-precip}$  values as increased summer precipitation. Our middle Holocene  $\Delta RH$  reconstruction average is +1% in comparison to modern, although as previously stated, the first half of the middle Holocene at Nuudsaku was likely wetter than the latter half.

Stansell et al. (2017) suggested that the generally higher  $\delta^{18}O_{calc}$  values during the middle Holocene may have been a result of higher temperatures or an increase in the amount of warm season precipitation. The mean middle Holocene CI-TJul value at Lake Nuudsaku is 18.0 °C, and we do not detect any statistically significant changes in that data set.

A reconstruction of July temperatures in a paleo-record from Laihalampi, Finland (Fig. 7) shows similar consistency in warm season temperatures. However, pollen proxies from the Baltic region covering the Holocene suggest that the summer temperatures in the Baltic region were the highest between ca 9500 to 4200 years BP (Renssen et al., 2012), and a reconstruction from Raigastvere (Estonia; Fig. 7) suggests that annual temperatures were more than 3 °C higher, and hydroclimate more arid in comparison to modern times (Seppä and Poska, 2004). The overall warm conditions were likely linked to strong anticyclonic blocking (Heikkilä and Seppä, 2010) which has been attributed to changes in solar insolation (Russo and Cubasch, 2016). This is also the most probable explanation for the relatively higher Norwegian Sea Surface Temperatures (SST) during the middle Holocene (Fig. 7). Based on our  $\varepsilon_{2Hterr/aq}$  proxy (Fig. 6), we suggest that about half of the middle Holocene between ~8000 and ~5800 cal yrs BP was wetter than present, with increased aridity thereafter.

Our reconstructed d-excess, which describes the environmental conditions at the moisture origin, shows relatively higher values ( $\sim$ -1‰) during the middle Holocene, which we interpret as relatively more northern/colder moisture source in comparison to the late Holocene ( $\sim$ -19‰). The higher d-excess values could be expected as there was probably less sea ice in the North (Bailey et al., 2021). This in concert with wet conditions inferred from  $\epsilon_{\rm 2Hterr/aq}$ , and generally higher  $\delta^2 H_{\rm paleo-precip}$  and  $\delta^{18} O_{\rm paleo-precip}$  values support overall increased summer precipitation, arriving from higher latitudes. We suggest that these conditions were particularly enhanced during three excursions in our un-smoothed data sets at 7800, 6900 and 6300 cal yrs BP when the  $\delta^2 H_{\rm paleo-precip}$  and d-excess values were higher in comparison to the rest of the middle Holocene.

#### 6.3. The 4.2 ka event

The period at around 4200 cal yrs BP, often referred to as the 4.2 ka climate anomaly (or event), has been identified as a time of abrupt changes in climate across the globe (Bradley and Bakke, 2019). As most of the proxy records during the event indicate relatively colder conditions, a few from Greenland suggest short-lived warmer conditions (Middleton, 2018; Bradley and Bakke, 2019 and the references therein). For example, Gkinis et al. (2014) demonstrated a warming signal in the NGRIP record at 4.2 ka. The pollen-based temperature reconstructions from Scandinavia argue that the general decrease in warm season insolation was responsible for an overall decrease in annual temperatures, however the time resolution of these proxies may not be high enough to detect such an abrupt event (Bradley and Bakke, 2019). The same study also suggested that the 4.2 ka climate anomaly was likely a result of changes in the Earth's atmosphere, and not the changing ocean circulation or solar forcing. They argue that there may have been anomalous trends in internal modes of variability which could have disrupted the local climate patterns. The Lake Nuudsaku unsmoothed ΔRH curve at 4200 cal yrs BP is significantly increased (13% above modern; Fig. 7), which is in an agreement with modeling results (Renssen, 2022). We also note the relatively higher unsmoothed d-excess value, which indicates that Nuudsaku precipitation originated from higher latitudes or colder sources during the 4.2 ka global anomaly (Fig. 7). Since the unsmoothed  $\varepsilon_{2Hterr/aq}$  data also indicates relatively more moist conditions, we suggest that the warm season during that brief time interval at Nuudsaku experienced increased wet conditions with northerly moisture origin.

# 6.4. The late Holocene

The late Holocene  $\delta^2 H_{paleo\text{-precip}}$  ( $-101\pm20\%$ ),  $\delta^{18} O_{paleo\text{-precip}}$  ( $-10.5\pm0.6\%$ ) and  $\epsilon_{2Hterr/aq}$  ( $-10.1\pm18\%$ ) values at Lake Nuudsaku between 4200 cal yrs BP and modern time suggest decreased summer

precipitation in comparison to the middle Holocene. The average  $\Delta RH$ reconstruction value for Lake Nuudsaku during the late Holocene was -5% in comparison to modern, indicating that the overall effective moisture content decreased. This also suggests that spring conditions in our study region could have become milder/warmer as it takes significantly less water vapor to saturate cold air in comparison to warm. We assume that the  $\delta^2 H_{C23}$  record is not significantly <sup>2</sup>H-enriched by transpiration, nor sensitive to evaporation. Therefore, the lower  $\delta^2 H_{\text{paleo}}$ precip values during the late Holocene may indicate a delay in the timing of spring meltwater, which would have left less time for warm season evapotranspiration. However, our late Holocene  $\epsilon_{2Hterr/aq}$  indicates more arid conditions (Fig. 7) prevailing at Nuudsaku. During modern times, the cold and dry conditions are associated with a negative phase of NAO, however we suggest decreased warm season precipitation at Nuudsaku during the late Holocene, and the modern-day NAO phases and precipitation amounts are only correlated during winter, not summer months. We note a brief excursion in our unsmoothed  $\Delta RH$  and  $\epsilon_{2Hterr/aq}$  curves at 3300 cal yrs BP when the effective moisture content was the lowest in our record, coinciding with the driest conditions. An increase in the CPI and an overall decrease in the n-alkane content at ~3000 cal yrs BP is likely linked to changes in land use as Poska et al. (2004) suggest an increase in agricultural practices and herding by human settlements. Another period with arid conditions occurred at 700 cal yrs BP. The  $\delta^2 H_{paleo-precip}$  values were increasing, suggesting higher summer precipitation, and the increasing d-excess more northerly sources from 700 cal yrs BP until modern. The same time period also shows wetter conditions in comparison to the preceding period between 5700 and 700 cal vrs BP.

The mean late Holocene CI-TJul at Lake Nuudsaku is 17.5 °C, with no statistically significant changes. The annual temperature reconstruction from Estonia (Seppä and Poska, 2004) suggests that the conditions became colder as the warm season insolation was decreasing (Fig. 7). This possibly shifted the local seasonality towards less extreme changes between winter and summer conditions as the annual temperatures in Estonia decreased over the Holocene (Fig. 7). The decreasing Atlantic SSTs in addition to modeling studies suggests that the westerly winds have weakened from the early Holocene until modern times (Grimalt and Marchal, 2006). Although our  $\varepsilon_{2\text{Hterr/aq}}$  proxy does indicate more arid conditions (which could be linked to a negative phase of the NAO, a positive phase of SCP, or a combination of these), our relatively lower late Holocene d-excess at suggests that the moisture probably originated from warmer sources in comparison to the middle Holocene.

# 7. Conclusions

In this study, we used sedimentary biomarkers with other proxies to reconstruct the hydroclimatic conditions in Estonia during the middle and late Holocene. We were able to use  $\delta^2H$  values from multiple biomarkers to quantify the relative humidity changes (ΔRH) at Lake Nuudsaku in relation to modern times, which was aided by estimates of the vegetation (pollen) composition of the lake catchment. We were also able to combine sediment-derived  $\delta^2 H_{paleo-precip}$  and  $\delta^{18} O_{paleo-precip}$ values from Lake Nuudsaku to examine hydroclimate changes recorded in both water isotope systems, and to combine them to calculate the dexcess. The relatively higher middle Holocene d-excess indicates that the precipitation most likely originated from northern latitudes. Conversely, the relatively lower average d-excess during the late Holocene implies more southerly dominating moisture sources. The middle Holocene period at Lake Nuudsaku was characterized by relatively higher  $\Delta RH$ (similar to today), higher variability in  $\delta^2 H_{paleo-precip}$ , and slightly higher warm season temperatures in comparison to the late Holocene. Our data demonstrates the possibility of warmer temperatures generally being accompanied by wetter conditions, which may prevail in the eastern Baltic region under future warming.

#### CRediT authorship contribution statement

Mariliis Eensalu: Conceptualization, Data curation, Formal analysis, Funding acquisition, Investigation, Methodology, Project administration, Resources, Software, Validation, Visualization, Supervision, Writing – original draft, review and editing. Daniel B. Nelson: Conceptualization, Data curation, Formal analysis, Investigation, Methodology, Validation, Supervision, Writing – original draft, review and editing. Anna Buczynska: Investigation, Data curation, analysis, Validation, Writing – original draft, review and editing. Oliver Rach: Formal analysis, Methodology, Validation, Writing – review & editing. Tomi P. Luoto: Formal analysis, Methodology, Validation, Writing – review & editing. Anneli Poska: Formal analysis, Methodology, Validation, Writing – review & editing. Nathan D. Stansell: Conceptualization, Funding acquisition, Resources, Software, Supervision, Writing – original draft, review and editing.

# Declaration of competing interest

The authors declare that they have no known competing financial interests or personal relationships that could have appeared to influence the work reported in this paper.

#### Data availability

The data tables can be found at 10.5281/zenodo.11214838.

#### Acknowledgements

We thank Dr. Dirk Sachse for help with the biomarker method development in the laboratory, and Dr. Jüri Vassiljev for the updated Lake Päidre age-depth scale. This work was supported by Erasmus+World program, Samuel S. Goldich and Carla Montgomery funds by the department of Earth, Atmosphere and Environment at Northern Illinois University, and Ann Mihkelson stipend by the Estonian National Culture Foundation awarded to ME. This project was also supported by the U.S. National Science Foundation, International Research Experiences for Students (IRES) grant (OISE-1827135). We thank one anonymous reviewer as well as Dr. Aaron Diefendorf for helpful feedback, and Dr. Antje Voelker for editorial handling of this manuscript.

# Appendix A. Supplementary data

Supplementary data to this article can be found online at https://doi.org/10.1016/j.quascirev.2024.108736.

# References

- Aemisegger, F., Pfahl, S., Sodemann, H., Lehner, I., Seneviratne, S.I., Wernli, H., 2014. Deuterium excess as a proxy for continental moisture recycling and plant transpiration. Atmos. Chem. Phys. 14 (8), 4029–4054.
- Aichner, B., Herzschuh, U., Wilkes, H., Vieth, A., Böhner, J., 2010. δD values of n-alkanes in Tibetan lake sediments and aquatic macrophytes - a surface sediment study and application to a 16ka record from Lake Koucha. Org. Geochem. 41, 779–790.
- Aichner, B., Hilt, S., Périllon, C., Gillefalk, M., Sachse, D., 2017. Biosynthetic hydrogen isotopic fractionation factors during lipid synthesis in submerged aquatic macrophytes: effect of groundwater discharge and salinity. Org. Geochem. 113, 10–16.
- Altabet, M.A., Francois, R., 1994. Sedimentary nitrogen isotopic ratio as a recorder for surface ocean nitrate utilization. Global Biogeochem. Cycles 8, 103–116.
- Bailey, H., Hubbard, A., Klein, E.S., Mustonen, K.R., Akers, P.D., Marttila, H., Welker, J. M., 2021. Arctic sea-ice loss fuels extreme European snowfall. Nat. Geosci. 14, 283–288.
- Barnston, A.G., Livezey, R.E., 1987. Classification, seasonality and persistence of low-frequency atmospheric circulation patterns. Mon. Weather Rev. 115, 1083–1126. Berke, M.A., Cartagena Sierra, A., Bush, R., Cheah, D., O'Connor, K., 2019. Controls on
- Berke, M.A., Cartagena Sierra, A., Bush, R., Cheah, D., O'Connor, K., 2019. Controls o leaf wax fractionation and δ2H values in tundra vascular plants from western Greenland. Geochem. Cosmochim. Acta 244, 565–583.

- Blaauw, M., Christen, J.A., 2018. RBacon: Age-Depth Modelling Using Bayesian Statistics. R package version 2.3.4. https://CRAN.R-project.org/package=r bacon1-14.
- Bonfils, C., de Noblet-Ducoudré, N., Guiot, J., Bartlein, P., 2004. Some mechanisms of mid-Holocene climate change in Europe, inferred from comparing PMIP models to data. Clim. Dyn. 23 (1), 79–98.
- Bova, S., Rosenthal, Y., Liu, Z., Godad, S.P., Yan, M., 2021. Seasonal origin of the thermal maxima at the Holocene and the last interglacial. Nature 589 (7843), 548–553.
- Bracegirdle, T.J., Colleoni, F., Abram, N.J., Bertler, N.A., Dixon, D.A., England, M., Favier, V., Fogwill, C.J., Fyfe, J.C., Goodwin, I., Goosse, H., 2019. Back to the future: using long-term observational and paleo-proxy reconstructions to improve model projections of Antarctic climate. Geosci. 9 (6), 255.
- Brader, A.V., van Winden, J.F., Bohncke, S.J.P., Beets, C.J., Reichart, G.J., de Leeuw, J. W., 2010. Fractionation of hydrogen, oxygen and carbon isotopes in n-alkanes and cellulose of three Sphagnum species. Org. Geochem. 41, 1277–1284.
- Bradley, R.S., Bakke, J., 2019. Is there evidence for a 4.2 ka BP event in the northern North Atlantic region? Clim. Past 15 (5), 1665–1676.
- Bray, E.E., Evans, E.D., 1961. Distribution of n-paraffins as a clue to recognition of source beds. Geochem. Cosmochim. Acta 22, 2–15.
- Brenner, M., Whitmore, T.J., Curtis, J.H., Hodell, D.A., Schelske, C.L., 1999. Stable isotope (δ13C and δ15N) signatures of sedimented organic matter as indicators of historic lake trophic state. J. Paleolimnol. 22, 205–221.
- Brooks, S.J.J., Langdon, P.G.G., Heiri, O, Heiri, O., 2007. The Identification and Use of Palaearctic Chironomidae Larvae in Palaeoecology. Quaternary Research Association, p. 276.
- Bush, R., McInerney, F., 2013. Leaf Wax N-Alkane Distributions in and across Modern Plants: Implications for Paleoecology and Chemotaxonomy, vol. 117. Elsevier, pp. 161–179.
- Cernusak, L.A., Barbour, M.M., Arndt, S.K., Cheesman, A.W., English, N.B., Feild, T.S., Helliker, B.R., Holloway-Phillips, M.M., Holtum, J.A.M., Kahmen, A., Mcinerney, F. A., Munksgaard, N.C., Simonin, K.A., Song, X., Stuart-Williams, H., West, J.B., Farquhar, G.D., 2016. Stable isotopes in leaf water of terrestrial plants. Plant Cell Environ. 39 (5), 1087–1102.
- Charman, D.J., Barber, K.E., Blaauw, M., Langdon, P.G., Mauquoy, D., Daley, T.J., Hughes, P.D.M., Karofeld, E., 2009. Climate drivers for peatland palaeoclimate records. Ouat. Sci. Rev. 28, 1811–1819.
- Colcord, D.E., Shilling, A.M., Sauer, P.E., Freeman, K.H., Njau, J.K., Stanistreet, I.G., Stollhofen, H., Schick, K.D., Toth, N., Brassell, S.C., 2018. Sub-Milankovitch paleoclimatic and paleoenvironmental variability in East Africa recorded by Pleistocene lacustrine sediments from Olduvai Gorge, Tanzania. Palaeogeogr. Palaeoclimatol. Palaeoccol. 495. 284–291.
- Coplen, T.B., 2011. Guidelines and recommended terms for expression of stable-isotoperatio and gas-ratio measurement results. Rapid Commun. Mass Spectrom. 25, 2538–2560.
- Corcoran, M.C., Thomas, E.K., Morrill, C., 2021. Using a paired chironomid  $\delta 180$  and aquatic leaf wax  $\delta 2H$  approach to reconstruct seasonality on western Greenland during the holocene. Paleoceanogr. Paleoclimatol. 36, 1–18.
- Dansgaard, W., 1964. Stable isotopes in precipitation. Tellus 16, 436-468.
- Diefendorf, A.F., Freeman, K.H., Wing, S.L., Graham, H.V., 2011. Production of n-alkyl lipids in living plants and implications for the geologic past. Geochem. Cosmochim. Acta 75, 7472–7485.
- Eensalu, M., Nelson, D.B., Buczynska, A., Rach, O., Klein, E.S., Dodd, J.P., Poska, A., Stansell, N.D., 2023. Hydrogen isotope biogeochemistry of plant waxes in paired lake catchments. Org. Geochem. 185, 104674.
- Eglinton, G., Hamilton, R.J., 1967. Leaf epicuticular waxes. Science 156, 1322–1335.
  Feakins, S.J., 2013. Pollen-corrected leaf wax D/H reconstructions of northeast African hydrological changes during the late Miocene. Palaeogeogr. Palaeoclimatol.
  Palaeoecol. 374. 62–71.
- Felde, V.A., Birks, H.H., 2019. Using species attributes to characterize late-glacial and early-Holocene environments at Kråkenes, western Norway. J. Veg. Sci. 30, 1228–1238.
- Feng, X., Faiia, A.M., Posmentier, E.S., 2009. Seasonality of isotopes in precipitation: A global perspective. J. Geophys. Res. 114 (D8).
- Ficken, K.J., Li, B., Swain, D.L., Eglinton, G., 2000. An n-alkane proxy for the sedimentary input of submerged/floating freshwater aquatic macrophytes. Org. Geochem. 745–749.
- Gao, L., Hou, J., Toney, J., MacDonald, D., Huang, Y., 2011. Mathematical modeling of the aquatic macrophyte inputs of mid-chain n-alkyl lipids to lake sediments: implications for interpreting compound specific hydrogen isotopic records. Geochem. Cosmochim. Acta 75, 3781–3791.
- Gat, J.R., 1996. Oxygen and hydrogen isotopes in the hydrologic Cycle. Annu. Rev. Earth Planet Sci. 24, 225–262.
- Giesecke, T., Bjune, A.E., Chiverrell, R.C., Seppä, H., Ojala, A.E.K., Birks, H.J.B., 2008. Exploring Holocene continentality changes in Fennoscandia using present and past tree distributions. Quat. Sci. Rev. 27, 1296–1308.
- Gimeno, L., Nieto, R., Drumond, A., Castillo, R., Trigo, R., 2013. Influence of the intensification of the major oceanic moisture sources on continental precipitation. Geophys. Res. Lett. 40, 1443–1450.
- Gkinis, V., Simonsen, S.B., Buchardt, S.L., White, J.W.C., Vinther, B.M., 2014. Water isotope diffusion rates from the NorthGRIP ice core for the last 16,000 years glaciological and paleoclimatic implications. Earth Planet Sci. Lett. 405, 132–141.
- Grimalt, J.O., Marchal, O., 2006. Age and alkenone-derived Holocene sea-surface temperature records of sediment core MD95-2015.
- Guiot, J., Harrison, S.P., Colin Prentice, I., 1993. Reconstruction of holocene precipitation patterns in europe using pollen and lake-level data. Quaternary Research 40, 139–149.

- Guo, D., Westra, S., Maier, H.R., 2016. An R package for modelling actual, potential and reference evapotranspiration. Environ. Model. Software 78, 216–224.
- Hammarlund, D., Barnekow, L., Birks, H.J.B., Buchardt, B., Edwards, T.W.D., 2002.
  Holocene changes in atmospheric circulation recorded in the oxygen-isotope stratigraphy of lacustrine carbonates from northern Sweden. Holocene 12, 339–351.
- Harris, D., Horwáth, W.R., van Kessel, C., 2001. Acid fumigation of soils to remove carbonates prior to total organic carbon or CARBON-13 isotopic analysis. Soil Sci. Soc. Am. J. 65, 1853–1856.
- Heikkilä, M., Seppä, H., 2010. Holocene climate dynamics in Latvia, eastern Baltic region: a pollen-based summer temperature reconstruction and regional comparison. Boreas 39, 705–719.
- Henderson-Sellers, A., McGuffie, K., Noone, D., Irannejad, P., 2004. Using stable water isotopes to evaluate basin-scale simulations of surface water budgets. J. Hydrometeorol. 5, 805–822.
- Herzschuh, U., Zhang, C., Mischke, S., Herzschuh, R., Mohammadi, F., Mingram, B., Kürschner, H., Riedel, F., 2005. A late Quaternary lake record from the Qillian Mountains (NW China): evolution of the primary production and the water depth reconstructed from macrofossil, pollen, biomarker, and isotope data. In: Global and Planetary Change, pp. 361–379.
- Hill, M.O., 1973. Diversity and evenness: a unifying notation and its consequences. Ecology 54, 427–432.
- Hurrell, J.W., Kushnir, Y., Ottersen, G., Visbeck, M., 2003. An overview of the north atlantic oscillation. Geophys. Monogr. 134, 1–35.
- Hurrell, J.W., Van Loon, H., 1997. Decadal variations in climate associated with the North Atlantic oscillation. Climatic Change 36, 301–326.
- Husson, F., Josse, J., Le, S., Mazet, J., 2016. FactoMineR: multivariate exploratory data analysis and data mining with R. http://cran.r-project.org/web/packages/Facto MineR/index.html.cran.rediris.es.
- IAEA, 2022. International atomic energy agency/world meteorological OrganizationGlobal Network of isotopes in precipitation. The GNIP Database. Retrieved from. https://nucleus.iaea.org/wiser.
- IPCC, 2019. Climate Change and Land: an IPCC special report. Climate Change and Land: an IPCC Special Report on climate change, desertification, land degradation, sustainable land management. food security, and greenhouse gas fluxes in terrestrial ecosystems 1–864.
- Ishiwatari, R., Negishi, K., Yoshikawa, H., Yamamoto, S., 2009. Glacial-interglacial productivity and environmental changes in Lake Biwa, Japan: a sediment core study of organic carbon, chlorins and biomarkers. Org. Geochem. 40, 520–530.
- Jaagus, J., 2009. Regionalisation of the precipitation pattern in the Baltic Sea drainage basin and its dependence on large-scale atmospheric circulation. Boreal Environ. Res. 14, 31–44.
- Jaagus, J., Ahas, R., 2000. Space-time variations of climatic seasons and their correlation with the phenological development of nature in Estonia. Clim. Res. 15, 207–219.
- Jones, H.G., 2013. Plants and microclimate: a quantitative approach to environmental plant physiology. Cambridge university press.Jouzel, J., Masson-Delmotte, V., Stiévenard, M., Landais, A., Vimeux, F., Johnsen, S.J.,
- Jouzel, J., Masson-Delmotte, V., Stiévenard, M., Landais, A., Vimeux, F., Johnsen, S.J., Sveinbjörnsdottir, A.E., White, J.W.C., 2005. Rapid deuterium-excess changes in Greenland ice cores: a link between the ocean and the atmosphere. Compt. Rendus Geosci. 337, 957–969.
- Keisling, B.A., Castañeda, I.S., Brigham-Grette, J., 2017. Hydrological and temperature change in Arctic Siberia during the intensification of Northern Hemisphere Glaciation. Earth Planet. Sci. Lett. 457, 136–148.
- Kim, S.T., Coplen, T.B., Horita, J., 2015. Normalization of stable isotope data for carbonate minerals: implementation of IUPAC guidelines. Geochem. Cosmochim. Acta 158, 276–289.
- Kim, S.T., O'Neil, J.R., 1997. Equilibrium and nonequilibrium oxygen isotope effects in synthetic carbonates. Geochem. Cosmochim. Acta 61, 3461–3475.
- Klein, E.S., Cherry, J.E., Young, J., Noone, D., Leffler, A.J., Welker, J.M., 2015. Arctic cyclone water vapor isotopes support past sea ice retreat recorded in Greenland ice. Sci. Rep. 5, 10295.
- Klein, E.S., Welker, J.M., 2016. Influence of sea ice on ocean water vapor isotopes and Greenland ice core records. Geophys. Res. Lett. 43, 12–475.
- Kopec, B.G., Feng, X., Posmentier, E.S., Sonder, L.J., 2019. Seasonal deuterium excess variations of precipitation at summit, Greenland, and their climatological significance. J. Geophys. Res. Atmos. 124, 72–91.
- Lamb, P.J., Peppler, R.A., 1987. North Atlantic oscillation: concept and an application. BULL. AM. METEOROL. SOC. 68, 1218–1225.
- Laugaste, R., Lessok, K., 2004. Planktonic algae and epiphyton of the littoral in Lake Peipsi, Estonia. Limnologica 34, 90–97.
- Laumets, L., Kalm, V., Poska, A., Kele, S., Lasberg, K., Amon, L., 2014. Palaeoclimate inferred from δ18O and palaeobotanical indicators in freshwater tufa of Lake Äntu Sinijärv, Estonia. J. Paleolimnol. 51, 99–111.
- Lauterbach, S., Brauer, A., Andersen, N., Danielopol, D.L., Dulski, P., Hüls, M., Milecka, K., Namiotko, T., Plessen, B., Grafenstein, U. Von, 2011. Multi-proxy evidence for early to mid-Holocene environmental and climatic changes in northeastern Poland. Boreas 40, 57–72.
- Leng, M.J., Marshall, J.D., 2004. Palaeoclimate interpretation of stable isotope data from lake sediment archives. Quat. Sci. Rev. 23, 811–831.
- Li, M., Hinnov, L., Kump, L., 2019. Acycle: time-series analysis software for paleoclimate research and education. Comput. Geosci. 127, 12–22.
- Luoto, T.P., Helama, S., 2010. Palaeoclimatological and palaeolimnological records from fossil midges and tree-rings: the role of the North Atlantic oscillation in eastern Finland through the medieval climate anomaly and little ice age. Quat. Sci. Rev. 29, 2411–2423.

- Luoto, T.P., Henriikka Kivilä, E., Kotrys, B., Plóciennik, M., Rantala, M.V., Nevalainen, L., 2020. Air temperature and water level inferences from northeastern Lapland (69°N) since the Little Ice Age. Pol. Polar Res. 41, 23–40.
- Luoto, T.P., Kotrys, B., Pióciennik, M., 2019. East European chironomid-based calibration model for past summer temperature reconstructions. Clim. Res. 77, 63–76.
- Luoto, T.P., Nevalainen, L., 2009. Larval chaoborid mandibles in surface sediments of small shallow lakes in Finland: implications for palaeolimnology. Palaeolimnological Proxies as Tools of Environmental Reconstruction in Fresh Water, pp. 185–195.
- Mäemets, A., 1968. Eesti Järved [Lakes of Estonia]. Valgus, Tallinn.
- Mätlik, O., Post, P., 2008. Synoptic weather types that have caused heavy precipitation in Estonia in the period 1961-2005. Est. J. Eng. 14, 195–208.
- Mauri, A., Davis, B.A.S., Collins, P.M., Kaplan, J.O., 2014. The influence of atmospheric circulation on the mid-Holocene climate of Europe: a data-model comparison. Clim. Past 10, 1925–1938.
- Meckler, A.N., Schubert, C.J., Cowie, G.L., Peiffer, S., Dittrich, M., 2004. New organic matter degradation proxies: valid in lake systems? Limnol. Oceanogr. 49, 2023–2033.
- Mellat, M., Bailey, H., Mustonen, K.R., Marttila, H., Klein, E.S., Gribanov, K., Bret-Harte, M.S., Chupakov, A.V., Divine, D.V., Else, B., Filippov, I., 2021. Hydroclimatic controls on the isotopic (δ18 O, δ2 H, d-excess) traits of pan-Arctic summer rainfall events. Front. Earth Sci. 9, 651731.
- Meyers, P.A., Lallier-Vergès, E., 1999. Lacustrine sedimentary organic matter records of Late Quaternary paleoclimates. J. Paleolimnol. 21, 345–372.
- Meyers, P.A., Teranes, J.L., 2001. Sediment organic matter. In: Tracking Environmental Change Using Lake Sediments. Kluwer Academic Publishers, pp. 239–269.
- Middleton, G.D., 2018. In: Harvey Weiss (Ed.), Megadrought and collapse: from early agriculture to Angkor. 2017, 92. Oxford University Press, Oxford, pp. 828–830, 978-0-19-932919-9£.
- Nelson, D.B., Basler, D., Kahmen, A., 2021. Precipitation isotope time series predictions from machine learning applied in Europe. Proc. Natl. Acad. Sci. 118 (26) e2024107118.
- Operstein, V., Frydman, S., 2000. The influence of vegetation on soil strength. Ground Improv. 4, 81–89.
- Pancost, R.D., Baas, M., Van Geel, B., Sinninghe Damsté, J.S., 2003. Response of an ombrotrophic bog to a regional climate event revealed by macrofossil, molecular and carbon isotopic data. Holocene 13, 921–932.
- Persoiu, A., Onac, B.P., Wynn, J.G., Blaauw, M., Ionita, M., Hansson, M., 2017. Holocene winter climate variability in Central and Eastern Europe. Scientific Reports 7 (1), 1–8.
- Pfahl, S., Sodemann, H., 2014. What controls deuterium excess in global precipitation? Clim. Past 10, 771–781.
- Poska, A., Saarse, L., Veski, S., 2004. Reflections of pre- and early-agrarian human impact in the pollen diagrams of Estonia. Palaeogeogr. Palaeoclimatol. Palaeoecol. 209, 37–50.
- Poynter, J., Eglinton, G., 1990. Molecular composition of three sediments from hole 717C: the Bengal Fan. Proc., scientific results, ODP, Leg 116, distal Bengal Fan 155–161.
- Puntsag, T., Mitchell, M.J., Campbell, J.L., Klein, E.S., Likens, G.E., Welker, J.M., 2016. Arctic Vortex changes alter the sources and isotopic values of precipitation in northeastern US. Sci. Rep. 6, 22647.
- Putman, A.L., Fiorella, R.P., Bowen, G.J., Cai, Z., 2019. A global perspective on local meteoric water lines: meta-analytic insight into fundamental controls and practical constraints. Water Resour. Res. 55, 6896–6910.
- Rach, O., Brauer, A., Wilkes, H., Sachse, D., 2014. Delayed hydrological response to Greenland cooling at the onset of the Younger Dryas in western Europe. Nat. Geosci. 7, 109–112.
- Rach, O., Kahmen, A., Brauer, A., Sachse, D., 2017. A dual-biomarker approach for quantification of changes in relative humidity from sedimentary lipid D/H ratios. Clim. Past 13, 741–757.
- Raidla, V., Kern, Z., Pärn, J., Babre, A., Erg, K., Ivask, J., Kalvāns, A., Kohán, B., Lelgus, M., Martma, T., Mokrik, R., Popovs, K., Vaikmäe, R., 2016. A δ18O isoscape for the shallow groundwater in the Baltic Artesian Basin. J. Hydrol. 542, 254–267.
- Räisänen, J., 2016. Future climate change in the baltic sea region and environmental impacts. Oxford Research Encyclopedia of Climate Science 1, 1–39.
- Reimer, P.J., Austin, W.E.N., Bard, E., Bayliss, A., Blackwell, P.G., Bronk Ramsey, C., Butzin, M., Cheng, H., Edwards, R.L., Friedrich, M., Grootes, P.M., Guilderson, T.P., Hajdas, I., Heaton, T.J., Hogg, A.G., Hughen, K.A., Kromer, B., Manning, S.W., Muscheler, R., Palmer, J.G., Pearson, C., Van Der Plicht, J., Reimer, R.W., Richards, D.A., Scott, E.M., Southon, J.R., Turney, C.S.M., Wacker, L., Adolphi, F., Büntgen, U., Capano, M., Fahrni, S.M., Fogtmann-Schulz, A., Friedrich, R., Köhler, P., Kudsk, S., Miyake, F., Olsen, J., Reinig, F., Sakamoto, M., Sookdeo, A., Talamo, S., 2020. The IntCal20 northern hemisphere radiocarbon age calibration curve (0-55 cal kBP). Radiocarbon 62, 725–757.
- Renssen, H., 2022. Climate model experiments on the 4.2 ka event: The impact of tropical sea-surface temperature anomalies and desertification. The Holocene 32 (5), 378–389.
- Renssen, H., Seppä, H., Crosta, X., Goosse, H., Roche, D.M., 2012. Global characterization of the holocene thermal maximum. Quat. Sci. Rev. 48, 7–19.
- Revelle, W., 1979. Hierarchical cluster analysis and the internal structure of tests. Multivariate Behav. Res. 14, 57–74.
- Rodionov, S.N., 2004. A sequential algorithm for testing climate regime shifts. Geophys. Res. Lett. 31, 2–5.
- Rosenzweig, C., Neofotis, P., 2013. Detection and attribution of anthropogenic climate change impacts. Wiley Interdisciplinary Reviews: Clim. Change 4, 121–150.

- Rummukainen, M., Räisänen, J., Bringfelt, B., Ullerstig, A., Omstedt, A., Willén, U., Hansson, U., Jones, C., 2001. A regional climate model for northern Europe: model description and results from the downscaling of two GCM control simulations. Clim. Dynam. 17, 339–359.
- Russo, E., Cubasch, U., 2016. Mid-to-late Holocene temperature evolution and atmospheric dynamics over Europe in regional model simulations. Clim. Past 12, 1645–1662.
- Saarse, L., Veski, S., Heinsalu, A., Rajamae, R., Martma, T., 1995. Litho- and biostratigraphy of Lake paidre, south Estonia. Proc. Est. Acad. Sci. Geol. 44, 45–59.
- Sachse, D., Billaulf, I., Bowen, G.J., Chikaraishi, Y., Dawson, T.E., Feakins, S.J., Freeman, K.H., Magill, C.R., McInerney, F.A., Van Der Meer, M.T.J., Polissar, P., Robins, R.J., Sachs, J.P., Schmidt, H.L., Sessions, A.L., White, J.W.C., West, J.B., Kahmen, A., 2012. Molecular paleohydrology: interpreting the hydrogen-isotopic composition of lipid biomarkers from photosynthesizing organisms. Annu. Rev. Earth Planet Sci. 40, 221–249.
- Sachse, D., Radke, J., Gleixner, G., 2004. Hydrogen isotope ratios of recent lacustrine sedimentary n-alkanes record modern climate variability. Geochem. Cosmochim. Acta 68, 4877–4889.
- Schimmelmann, A., Albertino, A., Sauer, P.E., Qi, H., Molinie, R., Mesnard, F., 2009. Nicotine, acetanilide and urea multi-level2H-,13C- and15N-abundance reference materials for continuous-flow isotope ratio mass spectrometry. Rapid Commun. Mass Spectrom. 23, 3513–3521.
- Schimmelmann, A., Lewan, M.D., Wintsch, R.P., 1999. D/H isotope ratios of kerogen, bitumen, oil, and water in hydrous pyrolysis of source rocks containing kerogen types I, II, IIS, and III. Geochim. Cosmochim. Acta 63 (22), 3751–3766.
- Seppä, H., Birks, H.J.B., Odland, A., Poska, A., Veski, S., 2004. A modern pollen-climate calibration set from northern Europe: developing and testing a tool for palaeoclimatological reconstructions. J. Biogeogr. 31, 251–267.
- Seppä, H., Poska, A., 2004. Holocene annual mean temperature changes in Estonia and their relationship to solar insolation and atmospheric circulation patterns. Quaternary Research 61, 22–31.
- Sharp, Z., 2007. Principles of stable isotope geochemistry. Choice Reviews Online 44, 44-6251.
- Stančikaite, M., Šeiriene, V., Kisieliene, D., Martma, T., Gryguc, G., Zinkute, R., Mažeika, J., Sinkunas, P., 2015. Lateglacial and early Holocene environmental dynamics in northern Lithuania: a multi-proxy record from Ginkunai Lake. Quat. Int. 357. 44–57.

- Stansell, N.D., Klein, E.S., Finkenbinder, M.S., Fortney, C.S., Dodd, J.P., Terasmaa, J., Nelson, D.B., 2017. A stable isotope record of Holocene precipitation dynamics in the Baltic region from Lake Nuudsaku, Estonia. Quat. Sci. Rev. 175, 73–84.
- Stivrins, N., Liiv, M., Brown, A., Banerjea, R.Y., Heinsalu, A., Veski, S., 2019. Investigating the impact of anthropogenic land use on a hemiboreal lake ecosystem using carbon/nitrogen ratios and coupled-optical emission spectroscopy. Palaeogeogr. palaeoclimatol. palaeoecol. 518, 1–9.
- Street-Perrott, F.A., Holmes, J.A., Robertson, I., Ficken, K.J., Koff, T., Loader, N.J., Marshall, J.D., Martma, T., 2018. The Holocene isotopic record of aquatic cellulose from Lake Äntu Sinijärv, Estonia: influence of changing climate and organic-matter sources. Quat. Sci. Rev. 193, 68–83.
- Surić, M., Columbu, A., Lončarić, R., Bajo, P., Bočić, N., Lončar, N., Drysdale, R.N., Hellstrom, J.C., 2021. Holocene hydroclimate changes in continental Croatia recorded in speleothem 813C and 818O from Nova Grgosova Cave. Holocene 31, 1401. 1416.
- Talbot, M.R., 1990. A review of the palaeohydrological interpretation of carbon and oxygen isotopic ratios in primary lacustrine carbonates. Chem. Geol. Isot. Geosci. 80, 261, 270
- Trenberth, K.E., 2011. Changes in precipitation with climate change. Clim. Res. 47,
- Veski, S., Seppä, H., Ojala, A.E.K., 2004. Cold event at 8200 yr B.P. recorded in annually laminated lake sediments in eastern Europe. Geology 32, 681–684.
- Walker, M.J.C., Berkelhammer, M., Björck, S., Cwynar, L.C., Fisher, D.A., Long, A.J., Lowe, J.J., Newnham, R.M., Rasmussen, S.O., Weiss, H., 2012. Formal subdivision of the holocene series/epoch: a discussion paper by a working group of intimate (integration of ice-core, marine and terrestrial records) and the subcommission on quaternary stratigraphy (international commission on stratigraphy). J. Quat. Sci. 27, 649-659
- Wang, M., Tan, B., 2020. Two types of the Scandinavian pattern: their formation mechanisms and climate impacts. J. Clim. 33, 2645–2661.
- Wanner, H., Beer, J., Bütikofer, J., Crowley, T.J., Cubasch, U., Flückiger, J., Goosse, H., Grosjean, M., Joos, F., Kaplan, J.O., Küttel, M., Müller, S.A., Prentice, I.C., Solomina, O., Stocker, T.F., Tarasov, P., Wagner, M., Widmann, M., 2008. Mid-to Late Holocene climate change: an overview. Quat. Sci. Rev. 27, 1791–1828.
- Xia, Z., Welker, J.M., Winnick, M.J., 2022. The seasonality of deuterium excess in non-polar precipitation. Glob. Biogeochem. Cycles 36 (10) e2021GB007245.